

MIT Open Access Articles

*Surface accretion of a pre-stretched
half-space: Biot's problem revisited*

The MIT Faculty has made this article openly available. **Please share**
how this access benefits you. Your story matters.

Citation: Rohan Abeyaratne, Eric Puntel, Filippo Recrosi, Giuseppe Tomassetti, Surface accretion of a pre-stretched half-space: Biot's problem revisited, Journal of the Mechanics and Physics of Solids, Volume 167, 2022, 104958.

As Published: 10.1016/j.jmps.2022.104958

Publisher: Elsevier BV

Persistent URL: <https://hdl.handle.net/1721.1/155202>

Version: Author's final manuscript: final author's manuscript post peer review, without publisher's formatting or copy editing

Terms of use: Creative Commons Attribution-Noncommercial-ShareAlike;Attribution-NonCommercial-ShareAlike 4.0 International





Surface accretion of a pre-stretched half-space: Biot's problem revisited

Rohan Abeyaratne^{a,1}, Eric Puntel^{b,1}, Filippo Recrosi^{c,1}, Giuseppe Tomassetti^{d,*,1}

^a Department of Mechanical Engineering, Massachusetts Institute of Technology, Cambridge, MA 02139, USA

^b Dipartimento Politecnico di Ingegneria e Architettura, Università di Udine, via del Cotonificio 114, Udine I-33100, Italy

^c Dipartimento di Ingegneria Strutturale e Geotecnica, Sapienza Università di Roma, Via Eudossiana 18, Roma, I-00184, Italy

^d Dipartimento di Ingegneria, Università degli Studi Roma Tre, via Vito Volterra 62, Roma I-00146, Italy

ARTICLE INFO

Keywords:

Actin
Stability
Surface growth
Half-space
Biot problem

ABSTRACT

Motivated by experiments on dendritic actin networks exhibiting surface growth, we address the problem of the stability of this growth process. We choose as a simple, reference geometry a biaxially stressed half-space growing at its boundary. The actin network is modeled as a neo-Hookean material. A kinetic relation between growth velocity and a stress-dependent driving force for growth is utilized. The stability problem is formulated and results are discussed for different loading and boundary conditions, with and without surface tension. Connections are drawn with Biot's 1963 surface instability threshold.

1. Introduction

In 1963 Biot showed that the equilibrium state of a half-space occupied by an incompressible neo-Hookean solid undergoing a homogeneous deformation with gradient

$$\bar{\mathbf{F}} = \begin{pmatrix} \lambda_1 & 0 \\ 0 & \lambda_2 \end{pmatrix}, \quad \lambda_1 \lambda_2 = 1, \quad (1)$$

with null body force and null traction on its surface, displays a bifurcation (see the cartoon in Fig. 1) when the tangential stretch λ_1 attains the critical value $\lambda_{\text{Biot}} \simeq 0.54$ defined as the unique real root of the equation $\lambda^3 + \lambda^2 + \lambda - 1 = 0$. This example leads to the expectation that when a finite block of rubber is compressed along its sides, undulations will form on its surface.

Biot's surface instability is, together with Euler's instability of the elastica, one of the few examples where the loss of stability of elastic equilibrium can be captured through elementary analytical arguments. Biot's surface instability is also regarded as particularly important in biomechanics because it provides a basis for the hypothesis that the folded shape developed by several organs during their growth may be the result of this kind of instability (see for example Li et al., 2012; Tallinen et al., 2013).

1.1. Stability of stress modulated growth

Work on biological growth has been pointing out that patterns observed during organ development may be the result of a more complicated type of instability which involves *feedback between growth and stress* (see for instance Garcia et al., 2018). Indeed, as

* Corresponding author.

E-mail addresses: rohan@mit.edu (R. Abeyaratne), eric.puntel@uniud.it (E. Puntel), filippo.recrosi@uniroma1.it (F. Recrosi), giuseppe.tomassetti@uniroma3.it (G. Tomassetti).

¹ All authors contributed equally to this work.

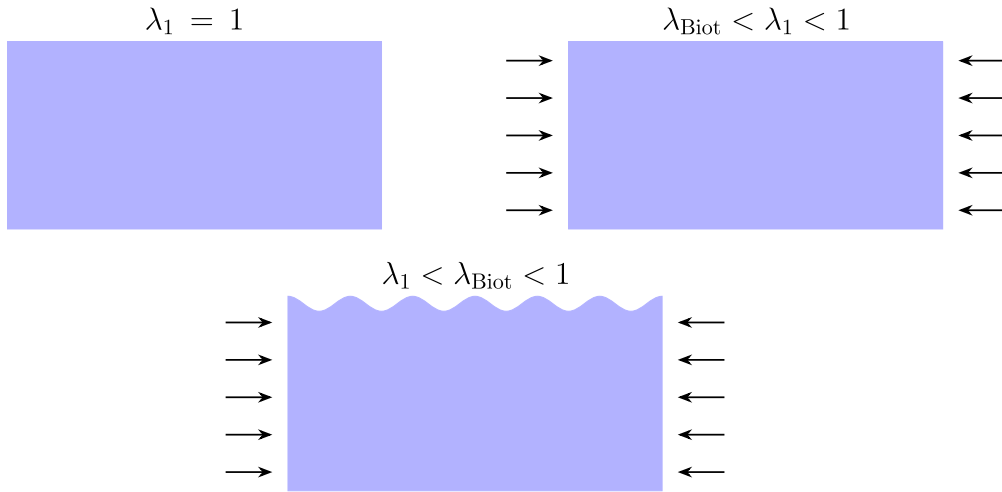


Fig. 1. Biot's surface instability. The critical value of the in-plane stretch is $\lambda_{\text{Biot}} \approx 0.54$.

discussed in Ambrosi et al. (2011), it is typical of biological tissues to regulate their growth according to mechanical cues from their environment. This results in the interplay between growth and stress. For example, in a confined environment growth typically leads to stress buildup, which in turn affects growth. This kind of interplay between growth and stress, often referred to as *stress-modulated growth*, is believed to play a key role not only for the development of organs, but also for pathological processes such as tumor growth (Ambrosi et al., 2012).

Still in biomechanics, but at the level of the individual cell, stress modulation is observed in the growth and remodeling of actin polymer networks, the main constituents of the cytoskeleton, as confirmed by *in vitro* experiments on growing actin networks acted upon by atomic-force microscopes (Bieling et al., 2016; Parekh et al., 2005) and by mathematical modeling (Cardamone et al., 2011; Abeyaratne and Purohit, 2020). In particular, a remarkable example of stress-driven growth instability is offered by experiments on a biomimetic system that replicates the self propulsion of *Listeria Monocytogenes*, Cameron et al. (1999), de Buyl et al. (2013). In its essence, this system consists of a micron-sized spherical bead whose surface is grafted with ActA, a protein found on the surface of *Listeria*, which promotes actin polymerization. When the bead is immersed in a water solution containing monomeric actin, a network grows on its surface; during accretion, the growing actin network accumulates residual stress (see Noireaux et al., 2000; Dafalias et al., 2008; Tomassetti et al., 2016) and an instability develops on its surface (see van der Gucht et al., 2005; Prost et al., 2008; John et al., 2008) to form a comet tail that pushes the bead inside the solution in a fashion similar to *Listeria*.

As noted by Erlich et al. (2019), capturing in mathematical terms the stability of stress-regulated growth is particularly challenging because of two main issues. First, there is still limited theoretical framework to help establish what growth law is more appropriate to model a certain biological system. Second, there is no general mathematical theory for the study of the stability of the ensuing system of partial differential equations, even in the quasistatic regime, *i.e.*, if inertial effects are neglected.

It is our opinion that the aforementioned difficulties are exacerbated in the case of surface growth, when accretion is localized at the boundary of the body. t

1.2. A variation on the theme of Biot's instability

In a previous contribution (Abeyaratne et al., 2020), motivated by the experimental work carried out by Parekh et al. (2005), Chaudhuri et al. (2007), and Bieling et al. (2016), we have been studying stress-modulated growth of a bar undergoing extension and capable of growing at its ends according to a kinetic law that draws into play the stress. Thanks to the choice of the one-dimensional geometry, by limiting our attention to the quasi-static regime we have been able to cast the governing equations in the form of a dynamical system and to carry out a complete stability analysis.

In the present paper we analyze a related problem constructed around a variation on the theme of Biot's instability, where the pre-stressed half-space is growing at its surface. This problem is inspired by the above-mentioned experimental and theoretical work on stress-driven instability of actin networks growing on rigid beads. Despite having in mind bodies made of polymerized actin immersed in solutions containing free actin monomers, our considerations apply to a generic material whose elementary constituents are dissolved in a surrounding fluid.

The *reference configuration* is a time dependent half-space $\Omega(t)$ bounded by a *growing surface* $\Gamma(t)$ (see Fig. 2) whose evolution obeys the *kinetic law*:

$$\chi(V) = f, \quad (2a)$$

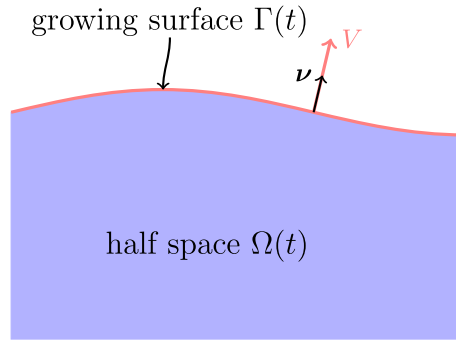


Fig. 2. The growing half-space in its reference configuration.

where V is the *outward normal velocity*, χ is a monotone increasing function satisfying $\chi(0) = 0$, and

$$f = \mathbf{F}\boldsymbol{\nu} \cdot \mathbf{S}\boldsymbol{\nu} + \mu - W(\mathbf{F}) \quad (2b)$$

is the thermodynamical force that drives growth. Such driving force depends on the boundary values of: the deformation gradient \mathbf{F} , the Piola stress \mathbf{S} , the outward unit normal $\boldsymbol{\nu}$, the strain energy $W(\mathbf{F})$, and on a constant μ , proportional to the difference between the chemical potential of the material in the dissolved state and solidified state. As a consequence of these assumptions, when the driving force f is positive, constituents dissolved in the solution attach to the surface. In this case, the normal velocity V is positive and $\Gamma(t)$ moves in the direction of $\boldsymbol{\nu}$. When f is negative, ablation takes place and elementary constituents at the surface of the body dissolve in the solution. As a consequence, V is negative and the boundary $\Gamma(t)$ moves inwards.

For a derivation of (2b) we refer to Tomassetti et al. (2016). For its generalization to situations when the boundary of the half-space carries surface energy we refer to Freund (1998) and to Fried and Gurtin (2003).

In Section 2 we combine the kinetic law (2) with the equations of nonlinear elastostatics, assuming plane strain, and we select three types of mechanical boundary conditions: a dead-load condition, a clamping condition, and a mixed condition. In the first case, the growing surface is subjected to a prescribed normal traction; in the second case, the growing surface is clamped on a flat support; in the third case, the growing surface is attached to a flat support, which allows it to slide tangentially without friction. These mechanical boundary conditions are motivated by the aforementioned work on the growth of actin on a rigid bead; in particular, clamping and mixed conditions are enforced on the surface of the bead, whereas null tractions are enforced on the external surface of the growing actin.

The result is a *free-boundary problem*, i.e., a system of partial differential equations to be solved not only for the deformation and the stress, but also for the growing surface $\Gamma(t)$. The free-boundary problem we study provides a paradigmatic model featuring feedback between surface growth and stress. If the body undergoes accretion or ablation at the boundary, the stress state must adapt to the change of the reference configuration; this adaptation, in turn, affects the growth rate at the boundary. Since inertia is being neglected, this feedback is “instantaneous”, but non-local in space.

1.3. The steady state and its stability

The free-boundary problem has a trivial solution, which we call the *steady state*, and which we denote by the overline notation $\bar{\cdot}$. In the steady state, the reference configuration is a half-space $\bar{\Omega}(t)$ with a flat boundary $\bar{\Gamma}(t)$ which translates vertically with constant velocity \bar{V} , as shown Fig. 3 (left). As in Biot’s example, the deformation is homogeneous, with gradient given by (1). However, unlike Biot, we assume that the pre-stress is biaxial. Thus, in addition to the tangential stretch λ_1 , we have the reactive pressure \bar{p} as control parameter. We assume that the half space is made of an incompressible neo-Hookean material. In terms of λ_1 and \bar{p} the Piola stress reads:

$$\bar{\mathbf{S}} = \begin{pmatrix} \bar{S}_{11} & 0 \\ 0 & \bar{S}_{22} \end{pmatrix} \quad \text{where} \quad \begin{aligned} \bar{S}_{11} &= G\lambda_1 - \bar{p}\lambda_1^{-1} \quad \text{and} \\ \bar{S}_{22} &= G\lambda_1^{-1} - \bar{p}\lambda_1. \end{aligned} \quad (3)$$

Consistent with (1), (2), and (3), the growth velocity \bar{V} is the unique solution (recall that χ is monotone increasing) of

$$\chi(\bar{V}) = \frac{1}{2}G(\lambda_1^{-2} - \lambda_1^2) + (G - \bar{p}) + \mu. \quad (4)$$

The growth velocity may be positive, null, or negative according to the particular choice of λ_1 and \bar{p} .

The bulk of this paper is addressed to the stability analysis of the steady state. With this aim, we linearize the free-boundary problem at the steady state to obtain an incremental problem. One of the unknowns appearing in the incremental problem is a function $\tilde{\zeta}(\tilde{\xi}_1, t)$ which describes the perturbation of the growing surface $\bar{\Gamma}(t)$ in the vertical direction, as shown schematically in Fig. 3 (right). The derivation of the incremental problem, which is carried out in Section 4, requires some care and effort; in our opinion this is one of the key contributions of the present paper.

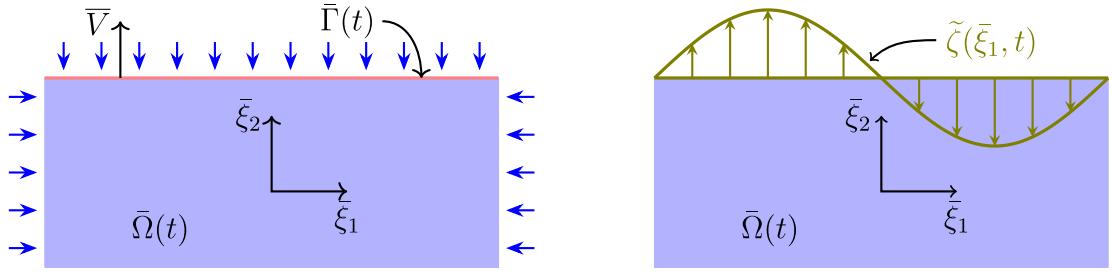


Fig. 3. Reference configuration for the steady state (left) and its perturbation (right).

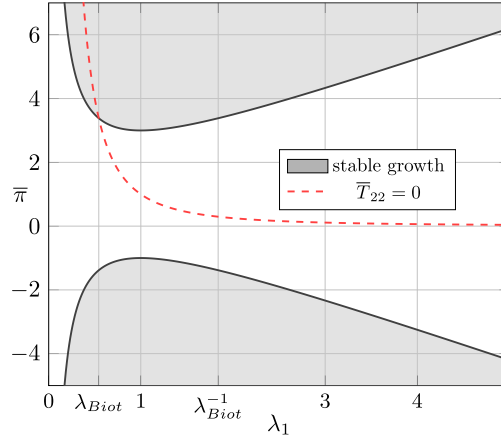


Fig. 4. Stability diagram on the $(\lambda_1, \bar{\pi})$ plane. The dashed curve corresponds to the case with the surface being traction free.

In Section 5 we carry out the stability analysis of the incremental problem. We show that the incremental problem admits solutions where the perturbation of the growing surface has the form

$$\tilde{\zeta}(\bar{\xi}_1, t) \propto \exp(\varphi t) \cos(\lambda_1 K \bar{\xi}_1), \quad \frac{\varphi}{K} = c \Phi(\lambda_1, \bar{\pi}), \quad (5)$$

where $\Phi(\lambda_1, \bar{\pi})$ is a dimensionless function whose expression depends on the imposed mechanical boundary conditions, and

$$\bar{\pi} = \frac{\bar{p}}{G} \quad \text{and} \quad c = \frac{G}{b}, \quad \text{with} \quad \bar{b} = \chi'(\bar{V}) > 0, \quad (6)$$

are, respectively, the *renormalized pressure*, and the *characteristic velocity related to growth*. Based on (5) we consider the steady state stable, at least within the class of perturbations considered here, if the growth exponent φ is negative.

When the growing surface is clamped to a flat support, surface growth is stable for all λ_1 and for all $\bar{\pi}$. If the support allows for sliding, stability holds for $\lambda_1 < 1/\lambda_{Biot}$. When the growing surface is unconstrained, but subjected to a dead load, the stability condition looks more complicated, and it is best illustrated through the diagram in Fig. 4, where states corresponding to stable growth are represented in gray and unstable states are represented in white.

In particular, the point $(\lambda_1, \bar{\pi}) = (1, 0)$ belongs to the unstable domain. In other words: the unstressed, load-free reference state is unstable with respect to growth.

It is possible, at least partially, to compare our results with those of the Biot problem by looking at the dashed curve in Fig. 4. The curve singles out in the $(\lambda_1, \bar{\pi})$ plane the set of states that correspond to null traction on the boundary, as originally considered by Biot. Remarkably, the intersection of this curve with the stability boundary is exactly for $\lambda_1 = \lambda_{Biot}$. A better comparison, however, requires to consider a generalization of Biot's problem to the case of biaxial stress state (see Appendix B). The discussion of this point is carried out in Section 5.4.

The extent of the white region in Fig. 4 is incompatible with experimental evidence on dendritic actin growth. For instance, the experiments on actin-based motility made by van der Gucht et al. (2005) suggest that the growth of actin networks is stable for moderate stretching.

Motivated by the intuitive expectation that surface tension may have a stabilizing effect, and in order to assess quantitatively such effect, we assume in Section 6 that the boundary of the half-space in the deformed configuration carries a surface energy σ . This assumption brings about the *elasto-capillary length*:

$$\ell = \frac{\sigma}{G}$$

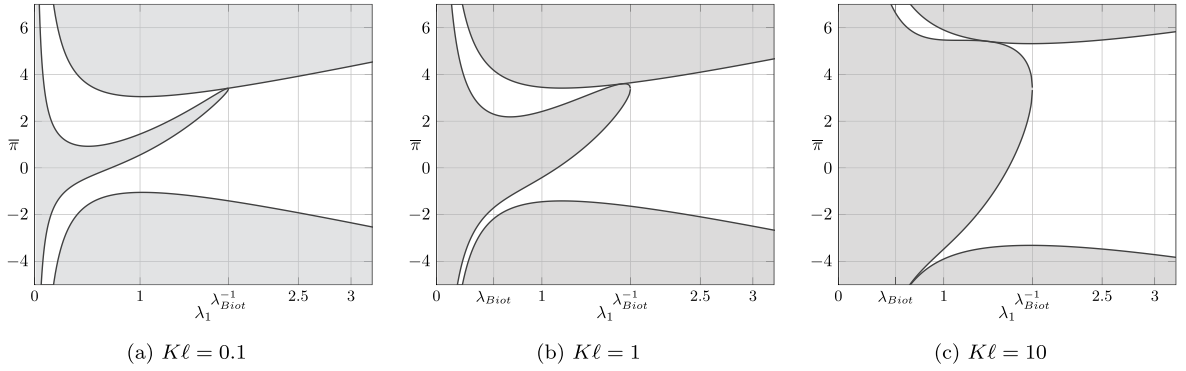


Fig. 5. Stability diagrams for the system with surface tension.

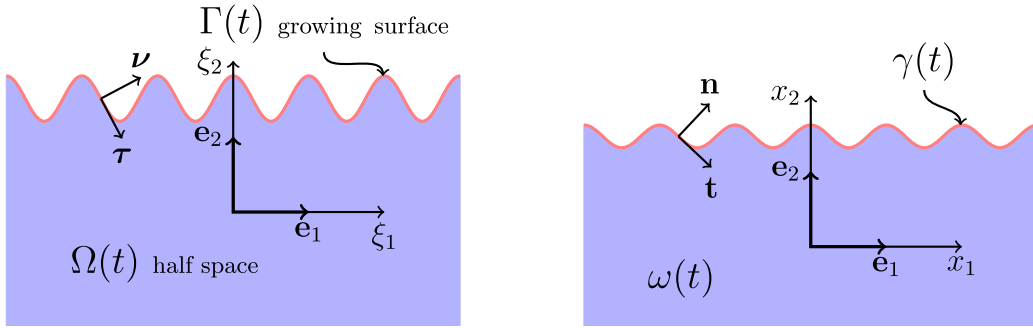


Fig. 6. Reference (left) and current (right) configuration of the growing elastic half space.

as a characteristic scale for the problem. By working out the ensuing calculations, we find solutions of the form

$$\tilde{\zeta}(\xi_1, t) \propto \exp(\varphi t) \cos(\lambda_1 K \xi_1), \quad \frac{\varphi}{K} = c\Psi(\lambda_1, \bar{\pi}, K\ell). \quad (7)$$

As expected, since the problem has a characteristic length ℓ , the growth exponent of a sinusoidal perturbation depends on the *renormalized wavenumber* $K\ell$. Three stability diagrams for increasing values of $K\ell$ are shown in Fig. 5. Compared with the case without surface tension, the stability diagrams contains a new stable domain whose extension is increasing with $K\ell$. In particular, each point of the $(\lambda_1, \bar{\pi})$ plane with $\lambda_1 < \lambda_{Biot}^{-1}$ is stable provided that the parameter $K\ell$ is sufficiently large, which corresponds to sufficiently small wavelengths (this shall be explained more in detail in Section 6). This result leads to the expectation that when the growing body is, instead of a half-space, a block of finite size where perturbations with a limited wavelength are admissible, the growth process is stable provided that surface tension is large enough. The quantitative evaluation of this effect is the other relevant contribution of the present paper.

2. The evolution problem

We adopt the plane strain assumption, and we work with a Cartesian coordinate system such that the generic position vector ξ in the reference configuration can be written as $\xi = \xi_1 \mathbf{e}_1 + \xi_2 \mathbf{e}_2$, where $\{\mathbf{e}_1, \mathbf{e}_2\}$ is the corresponding orthonormal basis.

During a generic evolution process, the elastic body occupies in its *reference configuration* the half-space:

$$\Omega(t) = \{(\xi_1, \xi_2) : \xi_2 < \zeta(\xi_1, t)\}. \quad (8)$$

The reference configuration $\Omega(t)$ is bounded from above by the growing surface $\Gamma(t)$ whose graph is $\zeta(\xi_1, t)$. We denote by ν and τ , respectively, the outward unit normal and the tangent to $\Gamma(t)$. In its *current configuration* the body occupies the half-space $\omega(t)$ bounded by the curve $\gamma(t)$, whose outward unit normal and unit tangent we denote, respectively, by \mathbf{n} and \mathbf{t} . The reference and the current configurations are sketched in Fig. 6.

2.1. Bulk equations

For the current configuration we introduce a Cartesian coordinate system (x_1, x_2) and we write $\mathbf{x} = x_1 \mathbf{e}_1 + x_2 \mathbf{e}_2$. With slight abuse of notation we use the symbol \mathbf{x} to denote both the typical point in the deformed configuration and the deformation $\mathbf{x} : \Omega(t) \mapsto \omega(t)$.

As usual, we denote by

$$\mathbf{F} := \text{grad}_{\mathbf{g}} \mathbf{x} \quad (9)$$

the deformation gradient. We assume that the material is an incompressible neo-Hookean solid, with strain energy given by

$$W(\mathbf{F}) = \frac{G}{2} (|\mathbf{F}|^2 - 2). \quad (10)$$

Incompressibility demands that the deformation gradient satisfies:

$$\det \mathbf{F} = 1 \quad \text{in } \Omega(t). \quad (11)$$

The Piola stress is therefore

$$\mathbf{S} := G \mathbf{F} - p \mathbf{F}^{-T}, \quad (12)$$

with p the reactive pressure. Neglecting body forces, the Piola stress obeys

$$\text{div}_{\mathbf{g}} \mathbf{S} = \mathbf{0} \quad \text{in } \Omega(t). \quad (13)$$

2.2. Mechanical boundary conditions

We shall consider three mechanical boundary conditions at Γ : a *dead-load* condition, a *clamping* condition, and a *mixed* condition.

Dead-load condition. This condition corresponds to the boundary $\Gamma(t)$ being free from constraints, and subjected to a fixed traction \mathbf{s} :

$$\mathbf{S} \mathbf{v} = \mathbf{s} \quad \text{on } \Gamma(t). \quad (14)$$

Clamping condition. This condition models a situation where growth takes place on a flat support. Since the material points that are being constrained may change from one time to another, there is some degree of arbitrariness in enforcing such a condition. We remove such arbitrariness by taking the boundary $\gamma(t)$ to be stationary. To simplify our mathematical developments we make the following choice of boundary condition:

$$x_1 = \xi_1, \quad x_2 = 0 \quad \text{on } \Gamma(t). \quad (15)$$

This condition enforces, in particular, that all points on the boundary stay on the line $x_2 = 0$. Thus, the surface $\gamma(t)$ coincides with $x_2 = 0$. Notice that, given the rigidity of the constraint, the horizontal stretch at the boundary is equal to 1.

Mixed condition. We model a frictionless flat support by prescribing the tangent shear traction to be zero, while keeping the normal component of the clamping condition:

$$\mathbf{S} \mathbf{v} \cdot \mathbf{e}_1 = 0, \quad x_2 = 0, \quad \text{on } \Gamma(t). \quad (16)$$

2.3. Growth processes

By a growth process we mean a smoothly-evolving triplet $t \mapsto (\Omega(t), \mathbf{x}(\cdot, t), p(\cdot, t))$ consisting of a reference configuration $\Omega(t)$, a deformation $\mathbf{x}(\cdot, t)$, and a pressure $p(\cdot, t)$ defined on $\Omega(t)$ such that the boundary $\Gamma(t)$ evolves according to the kinetic equation (2), the deformation gradient \mathbf{F} and the Piola stress \mathbf{S} defined, respectively, by (9) and (12) satisfy the incompressibility condition (11) and the force-balance equation (13), as well as one of the prescribed boundary conditions among (14), (15), and (16).

3. The steady state

Steady states have already been described in the Introduction. In this section we give their precise definition and we verify that this definition is consistent with the notion of growth process given in Section 2.3. Although the verification is trivial, it provides us with several formulas that we shall use in the linearization process in Section 4.

In brief, the steady state is defined as follows.

- (a) The reference configuration $\bar{\Omega}(t)$ is the half-space (see Fig. 7(a))

$$\bar{\Omega}(t) = \{\bar{\xi} = (\bar{\xi}_1, \bar{\xi}_2) : \bar{\xi}_2 < \bar{\zeta}(t)\}, \quad \bar{\zeta}(t) = \bar{V}t, \quad (17)$$

whose flat boundary

$$\bar{\Gamma}(t) = \{(\bar{\xi}_1, \bar{\xi}_2) : \bar{\xi}_2 = \bar{\zeta}(t)\}$$

translates in the vertical direction with constant velocity \bar{V} given by (4).

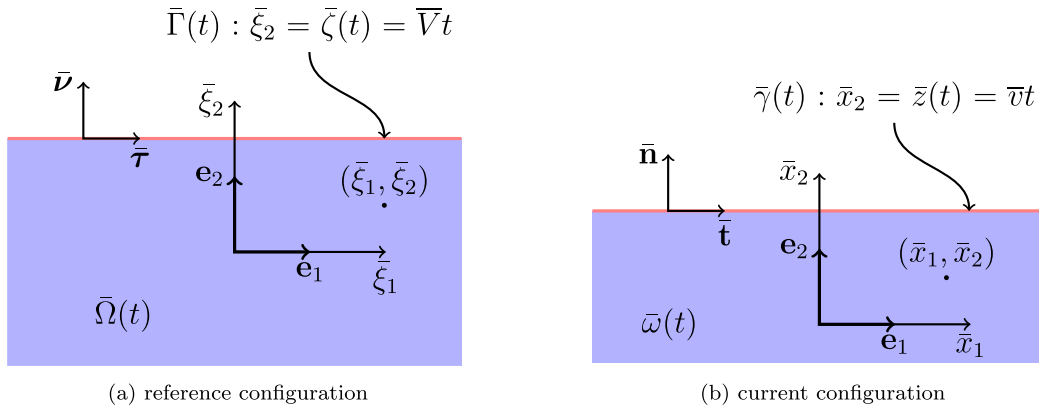


Fig. 7. Reference (left) vs. current (right) configuration in the steady state.

(b) The deformation $\bar{\mathbf{x}} : (\bar{\xi}_1, \bar{\xi}_2, t) \mapsto (\bar{x}_1, \bar{x}_2)$ is:

$$\bar{x}_1 = \lambda_1 \bar{\xi}_1, \quad \bar{x}_2 = \lambda_2 \bar{\xi}_2 + (\bar{v} - \lambda_2 \bar{V})t, \quad \lambda_2 = 1/\lambda_1, \quad (18a)$$

with

$$\bar{v} = \begin{cases} \lambda_2 \bar{V} & \text{in the dead-load case (14);} \\ 0 & \text{in the clamped (15) and mixed (16) cases,} \end{cases} \quad (18b)$$

and with $\lambda_1 = 1$ in the clamped case.

(c) the pressure \bar{p} is constant both in space and time.

The definition (18) may seem a bit twisted. However, (18) provides us with a single formula that accommodates all types of mechanical boundary conditions described in Section 2.2. Indeed, on substituting $\bar{\xi}_2 = \bar{\zeta}(t) = \bar{V}t$ in (18a) and on making use of (18b) we obtain $\bar{x}_2 = \bar{v}t$. This coordinate represents the vertical position of the boundary

$$\bar{\gamma}(t) = \{(\bar{x}_1, \bar{x}_2) : \bar{x}_2 = \bar{z}(t)\}, \quad \bar{z}(t) = \bar{v}t \quad (19)$$

of the deformed configuration

$$\bar{\omega}(t) = \{(\bar{x}_1, \bar{x}_2) : \bar{x}_2 < \bar{z}(t)\}. \quad (20)$$

Thus, in the clamped and mixed cases $\bar{z}(t) = 0$ and hence the boundary $\bar{\gamma}(t)$ of the deformed configuration coincides with $x_2 = 0$.

In the remaining part of this section we check that items (a)–(c) above define a growth process consistent with the notion given in Section 2.3. By (18) the deformation gradient is

$$\bar{\mathbf{F}} = \text{grad}_{\bar{\mathbf{x}}} \bar{\mathbf{x}} = \lambda_1 \mathbf{e}_1 \otimes \mathbf{e}_1 + \lambda_2 \mathbf{e}_2 \otimes \mathbf{e}_2. \quad (21)$$

By the constitutive equation (12), the Piola stress is

$$\bar{\mathbf{S}} = G\bar{\mathbf{F}} - \bar{p}\bar{\mathbf{F}}^{-T}. \quad (22)$$

Eqs. (21) and (22) are consistent, respectively, with (1) and (3). Since \bar{p} is constant, the bulk equations (11) and (13) are automatically satisfied. It thus remains for us to check that the growth velocity defined by (4) is consistent with the kinetic equation when deformation gradient and stress are given by (21) and (22), and that the mechanical boundary conditions are satisfied in the dead-load, clamped, and mixed cases.

The kinetic equation (2) reads

$$\chi(\bar{V}) = \bar{\mathbf{F}}\mathbf{e}_2 \cdot \bar{\mathbf{S}}\mathbf{e}_2 + \mu - W(\bar{\mathbf{F}}). \quad (23)$$

By (21) and (22), we have

$$\bar{\mathbf{F}}\mathbf{e}_2 = \lambda_1^{-1}\mathbf{e}_2, \quad \bar{\mathbf{S}}\mathbf{e}_2 = (G\lambda_1^{-1} - \bar{p}\lambda_1)\mathbf{e}_2. \quad (24)$$

Moreover, the strain energy (10) is

$$W(\bar{\mathbf{F}}) = \frac{G}{2}(\bar{\mathbf{F}} \cdot \bar{\mathbf{F}} - 2) = \frac{G}{2}(\lambda_1^2 + \lambda_1^{-2} - 2). \quad (25)$$

By combining (24) and (25) into (23) we obtain (4).

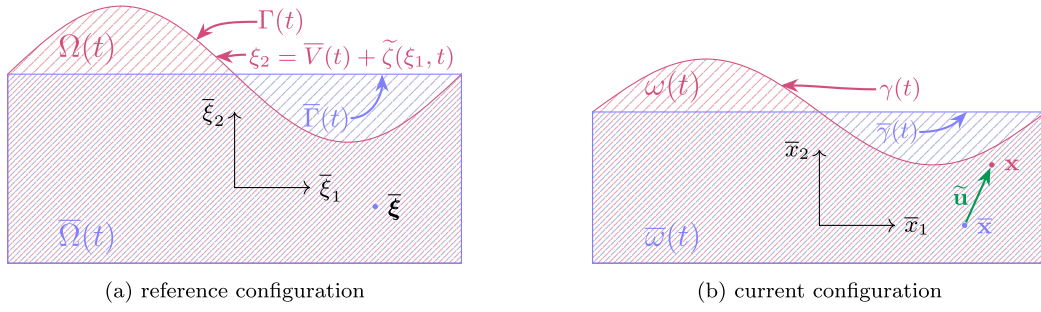


Fig. 8. The material point $\bar{\xi}$ occupies the position $\bar{\mathbf{x}}$ in the steady state and the position \mathbf{x} in the perturbed state. The points \mathbf{x} and $\bar{\mathbf{x}}$ are separated by the displacement $\tilde{\mathbf{u}}$.

We next verify the mechanical boundary conditions. In view of the second of (24), the dead-load condition (14) is satisfied provided that the boundary traction is $\mathbf{s} = \bar{\mathbf{j}}\mathbf{e}_2$, with

$$\bar{\mathbf{j}} = G\lambda_1^{-1} - \bar{p}\lambda_1. \quad (26)$$

Consistency with the clamping and mixed conditions is immediate.

We note that for λ_1 fixed, Eq. (26) puts the normal traction $\bar{\mathbf{j}}$ into one-to-one relation with \bar{p} . Thus, in the dead-load case we may use the pair $(\lambda_1, \bar{\mathbf{j}})$ instead of (λ_1, \bar{p}) as set of control parameters.

We record for later use the expression of the Cauchy stress

$$\bar{\mathbf{T}} = \bar{\mathbf{S}}\bar{\mathbf{F}}^T = G\bar{\mathbf{F}}\bar{\mathbf{F}}^T - \bar{p}\mathbf{I}, \quad (27)$$

where \mathbf{I} is the identity tensor. In components, we can write:

$$\bar{\mathbf{T}} = \begin{pmatrix} \bar{T}_{11} & 0 \\ 0 & \bar{T}_{22} \end{pmatrix}, \quad \text{with } \bar{T}_{ii} = G\lambda_i^2 - \bar{p}, \quad i = 1, 2. \quad (28)$$

4. The boundary-value problem governing perturbations

With a view towards assessing the stability of the steady state described in the previous section, we take this state as reference and we consider a perturbation of both the domain and of the fields of interest. We denote perturbed quantities by a tilde mark $\tilde{\cdot}$.

As depicted in Fig. 8(a), we describe a perturbation of $\bar{\Omega}(t)$ (the set defined in (17)) by adding a small, non-uniform change $\tilde{\zeta}(\xi_1, t)$ to the vertical coordinate $\bar{\zeta}(t)$ of its boundary. Specifically, we write the perturbed domain as

$$\Omega(t) = \left\{ \xi = (\xi_1, \xi_2) : \xi_2 < \bar{\zeta}(t) + \tilde{\zeta}(\xi_1, t) \right\}. \quad (29)$$

Concomitant with the perturbation of the reference configuration of the body, the positions of its material points are expected to undergo a change. In particular, if $\bar{\xi}$ is a material point that belongs to both the reference domain $\bar{\Omega}(t)$ and the perturbed domain $\Omega(t)$, then its position \mathbf{x} and pressure p in a perturbed state can be written in terms of a displacement $\tilde{\mathbf{u}}$ and pressure increment \tilde{q} as:

$$\mathbf{x} = \bar{\mathbf{x}} + \tilde{\mathbf{u}}; \quad p = \bar{p} + \tilde{q}. \quad (30)$$

For infinitesimal perturbations, $\Omega(t)$ collapses on $\bar{\Omega}(t)$ in the limit; as a result, $\tilde{\mathbf{u}}$ and \tilde{q} are incremental fields defined at every point $\bar{\xi}$ of the unperturbed reference configuration $\bar{\Omega}(t)$.

A standard approach when dealing with problems involving small displacements superposed on large deformations (see for example Fu and Ogden, 1999) is to think of the increments $\tilde{\mathbf{u}}$ and \tilde{q} as functions of the position $\bar{\mathbf{x}}$ that the material point $\bar{\xi}$ occupies in $\bar{\omega}(t)$. Consistent with this approach we shall also think of $\tilde{\zeta}$ as a scalar field defined on $\bar{\gamma}(t)$, rather than on $\bar{\Gamma}(t)$. In particular,

$$\frac{\partial \tilde{\zeta}}{\partial \bar{x}_1} = \frac{1}{\lambda_1} \frac{\partial \tilde{\zeta}}{\partial \xi_1} \quad (31)$$

In the remainder of this section, we perform a linearization of the bulk equations and of the boundary conditions and we derive a set of evolution equations and boundary conditions for the incremental fields $\tilde{\mathbf{u}}$, \tilde{q} , and $\tilde{\zeta}$.

By linearizing the bulk equations we get:

$$\left. \begin{aligned} \operatorname{div}_{\bar{\mathbf{x}}} \tilde{\mathbf{u}} &= 0 \\ \operatorname{div}_{\bar{\mathbf{x}}} \tilde{\mathbf{\Sigma}} &= 0 \\ \tilde{\mathbf{\Sigma}} &= \tilde{\mathbf{H}}\tilde{\mathbf{T}} + \bar{p}\tilde{\mathbf{H}} + \bar{p}\tilde{\mathbf{H}}^T - \tilde{q}\mathbf{I} \\ \tilde{\mathbf{H}} &:= \operatorname{grad}_{\bar{\mathbf{x}}} \tilde{\mathbf{u}} \end{aligned} \right\} \text{ in } \bar{\omega}(t). \quad (32)$$

By linearizing the kinetic equation we find:

$$\bar{b} \frac{\partial \tilde{\zeta}}{\partial t} - \tilde{\mathbf{S}} \mathbf{e}_2 \cdot \mathbf{e}_2 + \bar{T}_{11} \tilde{\mathbf{H}} \mathbf{e}_1 \cdot \mathbf{e}_1 = 0 \quad \text{on } \bar{\gamma}(t), \quad (33)$$

where $\bar{b} > 0$ is the incremental modulus defined in (6) and \bar{T}_{11} is the component of the Cauchy stress given in (28). By linearizing the mechanical boundary conditions we obtain:

$$\left. \begin{aligned} \tilde{\mathbf{S}} \mathbf{e}_2 - \lambda_2 \bar{T}_{11} \frac{\partial \tilde{\zeta}}{\partial \bar{x}_1} \mathbf{e}_1 &= \mathbf{0} && \text{for the dead-load case} \\ \tilde{\mathbf{u}} + \lambda_2 \tilde{\zeta} \mathbf{e}_2 &= \mathbf{0} && \text{for the clamped case} \\ \tilde{\mathbf{S}} \mathbf{e}_2 \cdot \mathbf{e}_1 - \lambda_2 \bar{T}_{11} \frac{\partial \tilde{\zeta}}{\partial \bar{x}_1} &= 0 && \text{for the mixed case} \\ \tilde{\mathbf{u}} \cdot \mathbf{e}_2 + \lambda_2 \tilde{\zeta} &= 0 && \end{aligned} \right\} \quad \text{on } \bar{\gamma}(t). \quad (34)$$

We wish to emphasize that, although in the original free-boundary problem the domain $\Omega(t)$ is unknown, its linearization at the steady state is formulated in the known (albeit time variable) domain $\bar{\omega}(t)$. In particular, the kinetic equation that rules growth is now reduced to a partial differential equation which holds on the boundary $\bar{\gamma}(t)$ of $\bar{\omega}(t)$.

4.1. Derivation of the linearized bulk equations (32)

The first two equations in system (32) are obtained, respectively, by linearizing the incompressibility condition (11) and the force-balance equation (13). As to the former, by differentiating both sides of the first of (30) with respect to $\tilde{\xi}$ and recalling that $\bar{\mathbf{F}} = \partial \bar{\mathbf{x}} / \partial \tilde{\xi}$, and by using the chain rule, we find that the deformation gradient in the perturbed state can be written as:

$$\mathbf{F} = \bar{\mathbf{F}} + \tilde{\mathbf{H}} \bar{\mathbf{F}}, \quad (35)$$

with $\tilde{\mathbf{H}}$ defined as in (32)₄. Thus, for every $\tilde{\xi} \in \bar{\Omega}(t)$, and for $\bar{\mathbf{x}}$ the corresponding image, the quantity

$$\tilde{\mathbf{F}}(\tilde{\xi}) = \tilde{\mathbf{H}}(\bar{\mathbf{x}}) \bar{\mathbf{F}} \quad (36)$$

is the increment of the deformation gradient at $\tilde{\xi}$. Thus, to within first order with respect to $\tilde{\mathbf{H}}$ the incompressibility condition (11), valid for both \mathbf{F} and $\bar{\mathbf{F}}$, yields

$$1 = \det \mathbf{F} = \det((\mathbf{I} + \tilde{\mathbf{H}}) \bar{\mathbf{F}}) = \det(\mathbf{I} + \tilde{\mathbf{H}}) \simeq \mathbf{I} + \text{tr } \tilde{\mathbf{H}} = 1 + \text{div}_{\bar{\mathbf{x}}} \tilde{\mathbf{u}}, \quad (37)$$

which leads to the first of (32).

We next turn our attention to the force-balance equation (13). Let $\tilde{\xi}$ be a material point that belongs to both $\bar{\Omega}(t)$ and $\Omega(t)$ (the reference configurations in the steady and perturbed states, respectively). Then we can define the *stress increment*:

$$\tilde{\mathbf{S}}(\tilde{\xi}) = \mathbf{S}(\tilde{\xi}) - \bar{\mathbf{S}}(\tilde{\xi}) \quad (38)$$

of the unperturbed Piola stress at the point $\tilde{\xi}$. If the perturbation is infinitesimal, the stress increment is defined at all points $\tilde{\xi}$ of $\bar{\Omega}(t)$. Then, since the stress is equilibrated in both the reference and the perturbed states, the incremental stress must satisfy:

$$\text{div}_{\tilde{\xi}} \tilde{\mathbf{S}} = \mathbf{0}. \quad (39)$$

The consideration we have made in the paragraph that follows (30), regarding the convenience of performing a change of independent variables for the fields $\tilde{\mathbf{u}}$ and \tilde{q} applies also to $\tilde{\mathbf{S}}$. However, since $\tilde{\mathbf{S}}$ is a flux, it is natural to push it forward from $\bar{\Omega}(t)$ to $\bar{\omega}(t)$ through the Piola transformation (see e.g. Gei and Ogden, 2002) associated to the homogeneous, isochoric deformation $\tilde{\xi} \mapsto \bar{\mathbf{x}}$. The result of this transformation is the tensor field $\tilde{\Sigma}$ defined by

$$\tilde{\Sigma}(\bar{\mathbf{x}}) := \tilde{\mathbf{S}}(\tilde{\xi}) \bar{\mathbf{F}}^T, \quad (40)$$

for all pairs $\bar{\mathbf{x}} \in \bar{\omega}(t)$ and $\tilde{\xi} \in \bar{\Omega}(t)$ related by (18a). It then follows that

$$\text{div}_{\bar{\mathbf{x}}} \tilde{\Sigma} = \mathbf{0}, \quad (41)$$

which is the second equation in (32). The third equation in (32) follows from the linearization of the constitutive equation (12) for the Piola stress. Indeed, from (35) we have, to first order with respect to $\tilde{\mathbf{H}}$, that $\mathbf{F}^{-1} \simeq \bar{\mathbf{F}}^{-1}(\mathbf{I} - \tilde{\mathbf{H}})$ and hence $\mathbf{F}^{-T} \simeq \bar{\mathbf{F}}^{-T} - \tilde{\mathbf{H}}^T \bar{\mathbf{F}}^{-T}$. By recalling (22), we can linearize the constitutive equation (12) as follows:

$$\mathbf{S} \simeq \bar{\mathbf{S}} + G \tilde{\mathbf{H}} \bar{\mathbf{F}} + \bar{p} \tilde{\mathbf{H}}^T \bar{\mathbf{F}}^{-T} - \tilde{q} \bar{\mathbf{F}}^{-T}. \quad (42)$$

This implies

$$\tilde{\mathbf{S}} \simeq G \tilde{\mathbf{H}} \bar{\mathbf{F}} + \bar{p} \tilde{\mathbf{H}}^T \bar{\mathbf{F}}^{-T} - \tilde{q} \bar{\mathbf{F}}^{-T}, \quad (43)$$

and hence

$$\tilde{\Sigma} \simeq G \tilde{\mathbf{H}} \bar{\mathbf{F}} \bar{\mathbf{F}}^T + \bar{p} \tilde{\mathbf{H}}^T - \tilde{q} \mathbf{I}. \quad (44)$$

By making use of (27) and (40), we obtain the third equation in (32).

4.2. Derivation of the linearized kinetic equation (33)

Eq. (33) follows from the linearization of the kinetic equation (2) at the steady state, where (23) holds. To carry out this linearization we fix a time t and a point $\xi \in \Gamma(t)$, and we rewrite the kinetic equation (2) as

$$\chi(V(\xi, t)) = \mathbf{F}(\xi, t) \mathbf{v}(\xi, t) \cdot \mathbf{S}(\xi, t) \mathbf{v}(\xi, t) + \mu - W(\mathbf{F}(\xi, t)). \quad (45)$$

By (29), we can write

$$\xi = (\bar{\xi}_1, \bar{\zeta}(t) + \tilde{\zeta}(\bar{\xi}_1, t)) \quad \text{for some } \bar{\xi}_1 \in \mathbb{R}. \quad (46)$$

We use an overbar for the horizontal coordinate of ξ to emphasize that ξ should be thought of as the result of the vertical translation, by an amount $\tilde{\zeta}(\bar{\xi}_1, t)$, of the point

$$\bar{\xi} = (\bar{\xi}_1, \bar{\zeta}(t)) \quad (47)$$

which belongs to $\bar{\Gamma}(t)$. We recall that the image of $\bar{\xi}$ under the homogeneous deformation (18a) lies on $\bar{\gamma}(t)$ and has coordinates

$$\bar{\mathbf{x}} = (\bar{x}_1, \bar{z}(t)), \quad \bar{x}_1 = \lambda_1 \bar{\xi}_1, \quad (48)$$

where \bar{z} is given by (18b) and (19)₂.

We now linearize the individual terms in (45). First, we consider the outward normal velocity. To approximate this quantity we introduce the function

$$g(\xi_1, \xi_2, t) := \bar{\zeta}(t) + \tilde{\zeta}(\xi_1, t) - \xi_2. \quad (49)$$

The growing surface $\Gamma(t)$ is the zero-level set of $g(\cdot, t)$, and the normal outward velocity is

$$V(\xi, t) = -\frac{\dot{g}(\xi, t)}{|\nabla g(\xi, t)|} = \frac{\bar{V} + \frac{\partial \tilde{\zeta}(\bar{\xi}_1, t)}{\partial t}}{\sqrt{1 + \left(\frac{\partial \tilde{\zeta}(\bar{\xi}_1, t)}{\partial \xi_1}\right)^2}} \simeq \bar{V} + \frac{\partial \tilde{\zeta}(\bar{\xi}_1, t)}{\partial t}, \quad (50)$$

to within first order with respect to the perturbation $\tilde{\zeta}$. Second, the outward unit normal is

$$\mathbf{v}(\xi, t) = -\frac{\nabla g(\xi, t)}{|\nabla g(\xi, t)|} = \frac{\mathbf{e}_2 - \frac{\partial \tilde{\zeta}(\bar{\xi}_1, t)}{\partial \xi_1} \mathbf{e}_1}{\sqrt{1 + \left(\frac{\partial \tilde{\zeta}(\bar{\xi}_1, t)}{\partial \xi_1}\right)^2}} \simeq \mathbf{e}_2 - \frac{\partial \tilde{\zeta}(\bar{\xi}_1, t)}{\partial \xi_1} \mathbf{e}_1. \quad (51)$$

Finally, assuming that the perturbed stress \mathbf{S} is sufficiently smooth, and on making use of (46), we can write

$$\begin{aligned} \mathbf{S}(\xi, t) &\simeq \mathbf{S}(\bar{\xi}, t) + \frac{\partial \mathbf{S}}{\partial \xi_2}(\bar{\xi}, t) \tilde{\zeta}(\bar{\xi}_1, t) \\ &\simeq \bar{\mathbf{S}} + \underbrace{\tilde{\mathbf{S}}(\bar{\xi}, t)}_{=0} + \underbrace{\frac{\partial \tilde{\mathbf{S}}}{\partial \xi_2}(\bar{\xi}, t) \tilde{\zeta}(\bar{\xi}_1, t)}_{\text{higher-order term}}. \end{aligned} \quad (52)$$

The third term on the right-hand side vanishes since $\bar{\mathbf{S}}$ is constant. The fourth term is of second order, and hence must be discarded in the linearization process. A similar argument applies to the deformation gradient, whose value in the reference state also does not depend on $\bar{\xi}$. Thus, we end up with:

$$\mathbf{S}(\xi, t) \simeq \bar{\mathbf{S}} + \tilde{\mathbf{S}}(\bar{\xi}, t), \quad \mathbf{F}(\xi, t) \simeq \bar{\mathbf{F}} + \tilde{\mathbf{F}}(\bar{\xi}, t) \quad \text{on } \bar{\Gamma}(t). \quad (53)$$

The same kind of linearization applies to the strain energy, and yields $W(\mathbf{F}(\xi, t)) \simeq W(\bar{\mathbf{F}}) + W'(\bar{\mathbf{F}}) \cdot \tilde{\mathbf{F}}(\bar{\xi}, t)$. In this last equation, since the increment $\tilde{\mathbf{F}}$ is consistent with the incompressibility constraint, the last term of the right-hand side of (54) is the work performed by the stress $\bar{\mathbf{S}}$ on $\tilde{\mathbf{F}}$. Thus,

$$W(\mathbf{F}(\xi, t)) = W(\bar{\mathbf{F}}) + \bar{\mathbf{S}} \cdot \tilde{\mathbf{F}}(\bar{\xi}, t). \quad (54)$$

On substituting (50)–(54) into (45) and retaining terms up to the first order we obtain:

$$\chi(\bar{V}) + \chi'(\bar{V}) \frac{\partial \tilde{\zeta}(\bar{\xi}_1, t)}{\partial t} \simeq \bar{\mathbf{F}} \mathbf{e}_2 \cdot \bar{\mathbf{S}} \mathbf{e}_2 + \mu - W(\bar{\mathbf{F}}) + \tilde{\mathbf{F}}(\bar{\xi}, t) \mathbf{e}_2 \cdot \bar{\mathbf{S}} \mathbf{e}_2 + \bar{\mathbf{F}} \mathbf{e}_2 \cdot \tilde{\mathbf{S}}(\bar{\xi}, t) \mathbf{e}_2 - \bar{\mathbf{S}} \cdot \tilde{\mathbf{F}}(\bar{\xi}, t). \quad (55)$$

A comparison with (23) allows us to identify the first order terms on both sides of (55) as:

$$\bar{b} \frac{\partial \tilde{\zeta}(\bar{\xi}_1, t)}{\partial t} = \tilde{\mathbf{F}}(\bar{\xi}, t) \mathbf{e}_2 \cdot \bar{\mathbf{S}} \mathbf{e}_2 + \bar{\mathbf{F}} \mathbf{e}_2 \cdot \tilde{\mathbf{S}}(\bar{\xi}, t) \mathbf{e}_2 - \bar{\mathbf{S}} \cdot \tilde{\mathbf{F}}(\bar{\xi}, t), \quad (56)$$

where $\bar{b} = \chi'(\bar{V})$. We now make use of (27), (31), (36), and (40) to obtain

$$\bar{b} \frac{\partial \tilde{\zeta}(\bar{x}_1, t)}{\partial t} = \tilde{\mathbf{H}}(\bar{\mathbf{x}}, t) \bar{\mathbf{F}} \mathbf{e}_2 \cdot \bar{\mathbf{S}} \mathbf{e}_2 + \bar{\mathbf{F}} \mathbf{e}_2 \cdot \tilde{\Sigma} \bar{\mathbf{F}}^T \mathbf{e}_2 - \bar{\mathbf{T}} \cdot \tilde{\mathbf{H}}(\bar{\mathbf{x}}, t). \quad (57)$$

We rewrite $\tilde{\mathbf{H}}\tilde{\mathbf{F}}\mathbf{e}_2 \cdot \tilde{\mathbf{S}}\mathbf{e}_2$ as $\lambda_2 \tilde{S}_{22} \tilde{H}_{22}$. Since $\lambda_2 \tilde{S}_{22} = \bar{T}_{22}$, the first term on the right-hand side of (57) is $\bar{T}_{22} \tilde{H}_{22}$. Furthermore, since $\tilde{\mathbf{F}}\mathbf{e}_2 = \lambda_2 \mathbf{e}_2$ and $\tilde{\mathbf{F}}^{-T} \mathbf{e}_2 = \lambda_2^{-1} \mathbf{e}_2$, we arrive at (33).

4.3. Derivation of the linearized mechanical boundary conditions (34)

To derive the linearization of the mechanical boundary conditions, we again fix our attention on a particular time t and a particular point ξ on the boundary $\Gamma(t)$, which we write as (46). We define $\bar{\xi}$ and $\bar{\mathbf{x}}$ as in (47) and (48).

Dead-load condition. Since the applied force is of dead-load type, the surface traction in the perturbed state is equal to that in the steady state. Thus, the Piola stress obeys $\mathbf{S}(\xi, t)\nu(\xi, t) = \bar{\mathbf{j}}\mathbf{e}_2$, where $\bar{\mathbf{j}}$ has been defined in (26). By making use of (24)₂, (26), (51), and (53), we find

$$\bar{\mathbf{j}}\mathbf{e}_2 = \mathbf{S}(\xi, t)\nu(\xi, t) \simeq (\bar{\mathbf{S}} + \tilde{\mathbf{S}}(\bar{\xi}, t))\left(\mathbf{e}_2 - \frac{\partial \tilde{\zeta}(\bar{\xi}_1, t)}{\partial \bar{\xi}_1} \mathbf{e}_1\right) \simeq \bar{\mathbf{j}}\mathbf{e}_2 + \tilde{\mathbf{S}}(\bar{\xi}, t)\mathbf{e}_2 - \frac{\partial \tilde{\zeta}(\bar{\xi}_1, t)}{\partial \bar{\xi}_1} \tilde{\mathbf{S}}\mathbf{e}_1. \quad (58)$$

Thus, to within first order, $\tilde{\mathbf{S}}(\bar{\xi}, t)\mathbf{e}_2 \simeq \frac{\partial \tilde{\zeta}(\bar{\xi}_1, t)}{\partial \bar{\xi}_1} \tilde{\mathbf{S}}\mathbf{e}_1$, and hence by (40) we have at the place $\bar{\mathbf{x}}$ defined by (48),

$$\tilde{\Sigma}(\bar{\mathbf{x}})\tilde{\mathbf{F}}^{-T}\mathbf{e}_2 \simeq \frac{\partial \tilde{\zeta}(\bar{\mathbf{x}}_1, t)}{\partial \bar{\mathbf{x}}_1} \tilde{\mathbf{S}}\mathbf{e}_1, \quad (59)$$

which gives the first of (34) where we have equality because both sides are of the same order.

Clamping condition. In this case, the coordinates of $\bar{\mathbf{x}}$ defined in (48) are $\bar{\mathbf{x}}_1 = \bar{\xi}_1$ and $\bar{\mathbf{x}}_2 = 0$ (see paragraph below (20)).

Let $\mathbf{x} = \mathbf{x}(\xi, t)$ be the position occupied by the material point ξ at time t . Since $\bar{\xi}$ is the vertical translation of ξ , it occupies the same position as ξ on the boundary, hence the coordinates of \mathbf{x} obey

$$x_1 = \bar{x}_1, \quad x_2 = 0. \quad (60)$$

By carrying out a similar calculation as in (52) we obtain

$$\begin{aligned} \mathbf{x}(\xi, t) &\simeq \mathbf{x}(\bar{\xi}, t) + \frac{\partial \mathbf{x}}{\partial \bar{\xi}_2}(\bar{\xi}, t) \tilde{\zeta}(\bar{\xi}_1, t) \\ &\simeq \bar{\mathbf{x}}(\bar{\xi}, t) + \tilde{\mathbf{u}}(\bar{\xi}, t) + \underbrace{\frac{\partial \bar{\mathbf{x}}}{\partial \bar{\xi}_2}(\bar{\xi}, t) \tilde{\zeta}(\bar{\xi}_1, t)}_{= \tilde{\mathbf{F}}\mathbf{e}_2} + \underbrace{\frac{\partial \tilde{\mathbf{u}}}{\partial \bar{\xi}_2}(\bar{\xi}, t) \tilde{\zeta}(\bar{\xi}_1, t)}_{\text{higher-order term}}. \end{aligned} \quad (61)$$

By writing (61) componentwise, we obtain

$$x_1 \simeq \bar{x}_1 + \underbrace{\tilde{\mathbf{u}}(\bar{\xi}, t) \cdot \mathbf{e}_1 + \tilde{\mathbf{F}}\mathbf{e}_2 \cdot \mathbf{e}_1}_{=0}, \quad x_2 \simeq \bar{x}_2 + \underbrace{\tilde{\mathbf{u}}(\bar{\xi}, t) \cdot \mathbf{e}_2 + \tilde{\mathbf{F}}\mathbf{e}_2 \cdot \mathbf{e}_2}_{= \lambda_2} \tilde{\zeta}(\bar{\xi}_1, t). \quad (62)$$

By making use of (60) and by expressing the incremental displacements in terms of variables in $\bar{\omega}(t)$ we obtain the second of (34).

Mixed condition. The linearization of the mixed condition leading to the third of (34) is obtained by a projection of the dead-load and the clamping conditions along \mathbf{e}_1 and \mathbf{e}_2 , respectively, followed by a linearization.

Remark. The linearization of the boundary conditions is more delicate than that of the bulk equations. Indeed, since the unperturbed domain $\bar{\Omega}(t)$ is an open set, any material point $\bar{\xi} \in \bar{\Omega}(t)$ is also a material point of the perturbed domain $\Omega(t)$, for a sufficiently small perturbation. This fact makes it possible to define infinitesimal increments of the fields of interest in all points of $\bar{\Omega}(t)$, and to derive the linearization of the bulk equations. A point $\bar{\xi}$ on the boundary of $\bar{\Omega}(t)$, on the other hand, may not be in $\bar{\Omega}(t)$, no matter how small the perturbation. This requires a slightly different procedure when it comes to constructing linear approximations of perturbed fields at the boundary (as in the case for the Piola stress in (52)). The result of this procedure, however, is the same as in the bulk if the field in question is spatially constant in the reference state (see for example the expressions of the Piola stress and deformation gradient in (53)).

5. Linear stability analysis

Renormalization. We shall work with renormalized quantities

$$\mathbf{u} = \frac{1}{L} \tilde{\mathbf{u}}, \quad q = \frac{\tilde{q}}{G}, \quad \zeta = \frac{\tilde{\zeta}}{L}, \quad T = \frac{\tilde{b}L}{G}, \quad \bar{\pi} = \frac{\tilde{p}}{G}, \quad (63)$$

where for consistency we introduce an arbitrary length L . We shall investigate the stability properties of the linearized system in terms of the two dimensionless parameters $(\lambda_1, \bar{\pi})$. We also introduce the independent variables

$$x_i = \frac{\bar{x}_i}{L}, \quad \tau = \frac{t}{T}. \quad (64)$$

We use the shorthand notation $\bullet_{,i} = \partial \bullet / \partial x_i$. We also use a superior dot to denote partial differentiation with respect to τ for x_1 and x_2 fixed.

In terms of dimensionless coordinates x_i and time τ , in the dead-load case the boundary has vertical coordinate

$$x_2 = z(\tau) = v\tau, \quad \text{where } v = \frac{T}{L}\bar{v}, \quad (65)$$

with \bar{v} defined in (23) and (18b). The quantities u_1 , u_2 , and q are the primary fields of the problem. By making use of (32)₃ and (32)₄, we rewrite (32)₁ and (32)₂ in component-wise form as

$$0 = u_{1,1} + u_{2,2}, \quad (66a)$$

$$q_{,1} = \lambda_1^2 u_{1,11} + \lambda_2^2 u_{1,22}, \quad (66b)$$

$$q_{,2} = \lambda_1^2 u_{2,11} + \lambda_2^2 u_{2,22}. \quad (66c)$$

The linearized kinetic equation (33) reads

$$\dot{\zeta} = -q - \lambda_1^2 u_{1,1} + \lambda_2^2 u_{2,2}. \quad (67)$$

By proceeding in a similar fashion, we derive the following set of boundary conditions from (34):

$$\left. \begin{aligned} u_{1,2} + \bar{\pi} \lambda_1^2 u_{2,1} - \lambda_1 (\lambda_1^2 - \bar{\pi}) \zeta_{,1} &= 0 \\ (\lambda_2^2 + \bar{\pi}) u_{2,2} - q &= 0 \end{aligned} \right\} \quad (\text{dead-load condition}),$$

$$\left. \begin{aligned} u_1 &= 0 \\ u_2 + \zeta &= 0 \end{aligned} \right\} \quad (\text{clamping condition}), \quad (68)$$

$$\left. \begin{aligned} u_{1,2} - \lambda_1^3 \zeta_{,1} &= 0 \\ u_2 + \lambda_2 \zeta &= 0 \end{aligned} \right\} \quad (\text{mixed condition}).$$

Conditions (68) hold on the horizontal line $x_2 = v\tau$, keeping in mind that $v = 0$ in the latter two cases. We recall that in the clamped case $\lambda_2 = \lambda_1 = 1$ (see the remark following (15)).

Although (68)₁ and (68)₅ follow from the same equation, namely, from the tangential component of the null traction condition (34)₁, in the mixed case the variable $\bar{\pi}$ drops out because $\zeta_{,1} = -u_{2,1} \lambda_2^{-1} = -u_{2,1} \lambda_1$ (by (68)₆). Note also that in writing the second clamping condition (68)₄ we have set $\lambda_2 = \lambda_1^{-1} = 1$.

Stream function and elimination of q and ζ . To begin with, we introduce a stream function $\psi(x_1, x_2, t)$ and we set

$$u_1 = \psi_{,2} \quad u_2 = -\psi_{,1}, \quad (69)$$

so that Eq. (66a) is automatically satisfied. Next, we eliminate the unknown pressure q from the bulk equations. Differentiation of (66b) w.r.t. x_2 , and of (66c) w.r.t. x_1 together with (69) allows the elimination of q and yields the partial differential equation

$$\lambda_1^4 \psi_{,1111} + (\lambda_1^4 + 1) \psi_{,1122} + \psi_{,2222} = 0 \quad (70)$$

which holds for all three boundary value problems.

In a similar fashion, we can eliminate the unknowns q and ζ from the boundary conditions by making use of the balance equation (66b) and of the kinetic equation (67). As a result, the mechanical boundary conditions (68) can be rewritten in terms of displacement, and then expressed in terms of the stream function:

$$\left. \begin{aligned} \psi_{,22} + \bar{v} \psi_{,222} - \bar{\pi} \lambda_1^2 (\psi_{,11} + \bar{v} \psi_{,112}) \\ + (\lambda_1^2 - \bar{\pi}) \lambda_1 ((2\lambda_1^2 + \lambda_2^2) \psi_{,112} + \lambda_2^2 \psi_{,222}) &= 0 \\ ((1 + \lambda_1^4) + \bar{\pi} \lambda_1^2) \psi_{,112} + \psi_{,222} &= 0 \end{aligned} \right\} \quad \text{for } x_2 = v\tau \quad (\text{dead-load condition})$$

$$\left. \begin{aligned} \psi_{,2} &= 0 \\ \psi_{,11} + \psi_{,222} &= 0 \end{aligned} \right\} \quad \text{for } x_2 = 0 \quad (\text{clamping condition}) \quad (71)$$

$$\left. \begin{aligned} \psi_{,22} + \lambda_1^3 ((2\lambda_1^2 + \lambda_2^2) \psi_{,112} + \lambda_2^2 \psi_{,222}) &= 0 \\ \lambda_1^3 \psi_{,11} + (1 + 2\lambda_1^4) \psi_{,112} + \psi_{,222} &= 0 \end{aligned} \right\} \quad \text{for } x_2 = 0 \quad (\text{mixed condition})$$

As emphasized in the above equations, the clamping and mixed conditions are imposed on the fixed set $x_2 = 0$. The scalar components (71)_{1,2} of the dead-load condition, on the other hand, are imposed on the moving set $x_2 = v\tau$. Because of this fact, the derivation of (71)_{1,2} is more subtle and deserves some detail. First, we rewrite (68)_{1,2} by making it explicit that τ appears in two arguments:

$$\lambda_2 u_{1,2}(x_1, v\tau, \tau) + \bar{\pi} \lambda_1 u_{2,1}(x_1, v\tau, \tau) - \zeta_{,1}(x_1, \tau) (\lambda_1^2 - \bar{\pi}) = 0, \quad (72)$$

$$(\lambda_2^2 + \bar{\pi}) u_{2,2}(x_1, v\tau, \tau) - q(x_1, v\tau, \tau) = 0.$$

Next, we differentiate (72)₁ with respect to τ , holding x_1 fixed and (72)₂ with respect to x_1 holding τ fixed, to obtain:

$$\lambda_2 (\dot{u}_{1,2} + v u_{1,22}) + \bar{\pi} \lambda_1 (\dot{u}_{2,1} + v u_{2,12}) - \dot{\zeta}_{,1} (\lambda_1^2 - \bar{\pi}) = 0, \quad (73)$$

$$(\lambda_2^2 + \bar{\pi}) u_{2,21} - q_{,1} = 0.$$

By a similar procedure, from the kinetic equation (67) we obtain:

$$\dot{\zeta}_{,1} = -q_{,1} - \lambda_1^2 u_{1,11} + \lambda_2^2 u_{2,21}. \quad (74)$$

We can now eliminate the unknowns $\dot{\zeta}_{,1}$ and $q_{,1}$ from (73) by making use of (74) and (66b), and then employ the stream function introduced in (69) to obtain (71)_{1,2}. The other boundary conditions in (71) are obtained in a similar fashion. Note again that for the clamping case we have $\lambda_1 = \lambda_2 = 1$.

Separation of variables. We seek a solution of (70) with the boundary conditions (71) in the form

$$\psi(x_1, x_2, \tau) = h(y) g(\tau) e^{ikx_1}, \quad \text{with } y = k(x_2 - v\tau), \quad (75)$$

with $k > 0$ without loss of generality. Substituting the above Ansatz into the perturbed equilibrium PDE (70) yields an ODE for the function h :

$$h'''' - (\lambda_1^4 + 1)h'' + \lambda_1^4 h = 0 \quad \text{for } y < 0, \quad (76)$$

The characteristic equation of (76) has roots $\pm\lambda_1^2$ and ± 1 . Neglecting negative roots for which the perturbation blows up for $y \rightarrow -\infty$, the general expression for h is

$$h(y) = A e^y + B e^{\lambda_1^2 y}, \quad (77)$$

when $\lambda_1 \neq 1$. When $\lambda_1 = 1$, as in the clamped case, $+1$ becomes a double root and h takes the form

$$h(y) = (A + B y) e^y. \quad (78)$$

As far as the function $g(\tau)$ in (75) is concerned, compatibility with the boundary conditions (71) requires that $\dot{g}(\tau)$ be proportional to $g(\tau)$. Hence $g(\tau)$ is also exponential:

$$g(\tau) = e^{\phi\tau}. \quad (79)$$

Starting from the Ansatz (75), each of the three pairs of boundary conditions in (71) leads to a different problem, which is henceforth analyzed separately.

We note in passing that the choice $k > 0$ in (75) is not restrictive. Indeed, if we select $k < 0$ then the solution must be bounded for $y \rightarrow +\infty$, which leads us to taking the negative roots of the characteristic equation, instead of the positive ones. As a result, the solution is unchanged.

5.1. Dead-load case

We substitute the expressions (77) and (79) for $h(y)$ and $g(\tau)$ into the Ansatz (75). Then we impose the dead-load boundary conditions (71)₁ and (71)₂. In performing these calculations, it is useful to note that, by (75), we have $\dot{\psi} + v\psi_{,2} = \phi\psi$. The result is a linear system with respect to the amplitudes A and B , which, after some manipulation, can be written in matrix notation as follows

$$\begin{bmatrix} (1 + \bar{\pi}\lambda_1^2)\phi - 2\lambda_1^3(\lambda_1^2 - \bar{\pi})k & \lambda_1^2(\lambda_1^2 + \bar{\pi})\phi - \lambda_1(1 + \lambda_1^4)(\lambda_1^2 - \bar{\pi})k \\ \lambda_1^2 + \bar{\pi} & 1 + \bar{\pi}\lambda_1^2 \end{bmatrix} \begin{bmatrix} A \\ B \end{bmatrix} = \begin{bmatrix} 0 \\ 0 \end{bmatrix}. \quad (80)$$

Non trivial solutions are obtained when the determinant of the coefficient matrix is zero, that is when

$$\frac{\phi}{k} = \frac{\lambda_1(\lambda_1^2 - \bar{\pi})^2(\lambda_1^2 + 1)}{(1 + \lambda_1^2)^2 - \lambda_1^2(\bar{\pi} - 1)^2} =: \Phi(\lambda_1, \bar{\pi}). \quad (81)$$

By linearity, the boundary perturbation has the form:

$$\zeta(x_1, \tau) \propto e^{ikx_1} e^{\phi\tau}. \quad (82)$$

We now use (63) and we recall that $\bar{x}_1 = \lambda_1 \bar{\xi}_1$ to write

$$\tilde{\zeta}(\bar{\xi}_1, t) = L\zeta(x_1, \tau) = L\zeta\left(\frac{\lambda_1 \bar{\xi}_1}{L}, \frac{t}{T}\right) \propto \exp\left(i\frac{k\lambda_1}{L}\bar{\xi}_1\right) \exp\left(\frac{G\phi}{bL}t\right) = \exp(i\lambda_1 K \bar{\xi}_1) \exp(\varphi t), \quad (83)$$

where we have set

$$K = \frac{k}{L} \quad \text{and} \quad \varphi = \frac{G\phi}{bL}. \quad (84)$$

By (81), the growth exponent φ and the wavenumber K are related by

$$\varphi = \frac{Gk}{bL} \Phi(\lambda_1, \bar{\pi}) = \frac{G}{b} K \Phi(\lambda_1, \bar{\pi}). \quad (85)$$

We recover (5) by retaining the real part of (83).

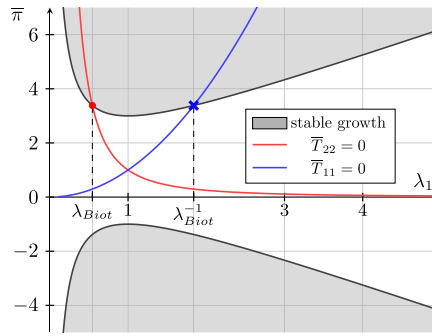


Fig. 9. Stability domains in the $\lambda_1 - \bar{\pi}$ plane for the dead-load case. The growth exponent is negative in the gray region and positive in the white region, with the exception of the curve $\bar{T}_{11} = 0$, where it vanishes.

5.2. Clamping case

Expressions (78) and (79) are substituted into (75) which is in turn inserted into the boundary conditions (71)_{3,4}. The thus obtained linear system of equations in the unknown coefficients A and B reads:

$$\begin{bmatrix} 1 & 1 \\ k - \phi & 3k \end{bmatrix} \begin{bmatrix} A \\ B \end{bmatrix} = \begin{bmatrix} 0 \\ 0 \end{bmatrix}. \quad (86)$$

By imposing the vanishing of the determinant we obtain

$$\frac{\phi}{k} = -2. \quad (87)$$

5.3. Mixed case

In this case the coefficient matrix has the form:

$$\begin{bmatrix} \phi - 2\lambda_1^5 k & \lambda_1^4 \phi - \lambda_1^3 (1 + \lambda_1^4) k \\ \lambda_1 \phi + 2\lambda_1^2 k & \lambda_1 \phi + (\lambda_1^4 + 1) k \end{bmatrix} \begin{bmatrix} A \\ B \end{bmatrix} = \begin{bmatrix} 0 \\ 0 \end{bmatrix} \quad (88)$$

Non trivial solutions occur when

$$\frac{\phi}{k} = \frac{\lambda_1^6 - 3\lambda_1^4 - \lambda_1^2 - 1}{\lambda_1 (\lambda_1^2 + 1)}. \quad (89)$$

5.4. Discussion

We discuss the results for each different boundary condition separately.

Dead-load case. From (81) we can determine the sign of ϕ . Then the $\lambda_1 - \bar{\pi}$ plane may be partitioned in two regions, as shown in Fig. 9, according to whether $\phi < 0$ (stable growth) and $\phi > 0$ (unstable growth).

Observe that the numerator of (81) is non-negative and it is the denominator that can change its sign. The stable and unstable regions are separated by the set of points defined by the equation

$$\bar{\pi} = 1 \pm \left(\lambda_1 + \frac{1}{\lambda_1} \right), \quad (90)$$

which comes from the denominator vanishing in (81).

The set defined by (90) consists of two curves arranged symmetrically about the horizontal line $\bar{\pi} = 1$. The growth exponent ϕ is positive in the white region and negative in the gray region, with the exception of the curve $T_{11} = 0$, where ϕ vanishes. The linear system (32)–(34), which governs incremental surface growth, has an exponentially growing solution for all pairs $(\lambda_1, \bar{\pi})$ in the white region shown in Fig. 9. We therefore conclude the following:

- The steady growth of a half-space subject to a dead load on its surface is unstable for all pairs $(\lambda_1, \bar{\pi})$ of in-plane stretch and renormalized pressure which lie in the white region of Fig. 9 delimited by the curves (90).

In the remaining set of points, corresponding to the gray region, the growth exponent is negative, hence the solutions constructed with the Ansatz (75) decay exponentially in time. We therefore consider the corresponding steady state to be stable.

To gain further insight we begin with the following observation:

- The two curves defined by (90), which delimit the white region in Fig. 9, are not curves of marginal stability, i.e., though $\phi > 0$ on one side, $\phi < 0$ on the other side, $\phi \neq 0$ on each such curve since it blows up.

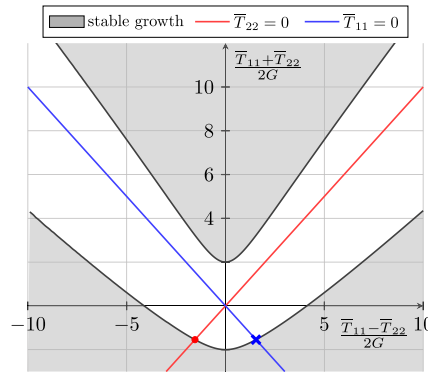


Fig. 10. Stability domains in the deviatoric vs mean stress plane.

In fact, the curves defined by (90) correspond to a singularity of $\Phi(\lambda_1, \bar{\pi})$. To better comprehend what happens when the curves defined by (90) are crossed, it is useful to consider a loading path with null dead load applied on the surface, which corresponds to $\bar{T}_{22} = 0$ by (28). This loading path corresponds to the curve $\bar{\pi} = 1/\lambda_1^2$, depicted in red in Fig. 9. Remarkably, this curve intersects the stability domain when $\lambda_1 = \lambda_{\text{Biot}}$, hence crossing the boundary of the domain of stable growth exactly when the conditions of *mechanical surface instability* is satisfied. Indeed, a plot of ϕ versus λ_1 would show a singularity at $\lambda_1 = \lambda_{\text{Biot}}$.

Similarly, in the case in which the half-space is stressed only in the \bar{x}_2 and not in the \bar{x}_1 direction, the condition $\bar{T}_{11} = 0$ corresponds to the curve $\bar{\pi} = \lambda_1^2$, depicted in blue in Fig. 9. Note that this curve is a zero of the function Φ defined in (81). This curve however does not correspond to marginal stability, but rather to a minimum of the number ϕ/k in the white region. The growth stability threshold is crossed in this case at $\lambda_1 = 1/\lambda_{\text{Biot}}$, i.e. $\lambda_2 = \lambda_{\text{Biot}}$.

The extension of Biot's original setup (without growth) to the case of non-vanishing normal dead-load traction (see the example worked out in Appendix B) shows that the curves defined by (90) correspond to a bifurcation of mechanical equilibrium. Hence, we observe an interesting “flipping”: in the purely mechanical case, i.e. without growth, the reference state is mechanically stable when the pair $(\lambda_1, \bar{\pi})$ is in the white region (which is unstable with respect to growth), and mechanically unstable when in the gray region (which is stable with respect to growth).

Given that in an experimental situation, the stress components at steady state may likely represent the control parameters, it is useful to express the stability domains in terms of \bar{T}_{11} and \bar{T}_{22} or better, as it turns out, in terms of the mean and deviatoric stresses. Let \bar{m} and \bar{d} be the steady state, non dimensional mean and deviatoric stress values respectively:

$$\bar{m} = \frac{\bar{T}_{11} + \bar{T}_{22}}{2G} \quad \text{and} \quad \bar{d} = \frac{\bar{T}_{11} - \bar{T}_{22}}{2G}. \quad (91)$$

Recalling that $\lambda_2 = \lambda_1^{-1}$ and using Eqs. (28) one obtains the following relations:

$$\lambda_1^2 = \sqrt{1 + \bar{d}^2} + \bar{d} \quad \text{and} \quad \bar{\pi} = \sqrt{1 + \bar{d}^2} - \bar{m}. \quad (92)$$

These relations deliver the boundary of the stability domains in terms of \bar{d} and \bar{m} once substituted into (90). The two domains are shown in gray in Fig. 10. They are symmetric with respect to the vertical non-dimensional mean stress axis. For $\bar{m} < -2$, growth is always stable. For $-2 < \bar{m} < 2$, growth is stable for both sufficiently large and small values of the deviatoric stress. For $\bar{m} > 2$, growth is stable for sufficiently small and large values of the deviatoric stress. The uniaxial loading paths $\bar{T}_{22} = 0$ and $\bar{T}_{11} = 0$ are also displayed in Fig. 10 and appear as straight lines crossing the stability domain at $\bar{m} = |\bar{d}| = \lambda_{\text{Biot}}^2 - 1/\lambda_{\text{Biot}}^2$.

Clamping case. From the result obtained in Section 5.2, in the clamping case, surface growth is always stable. This mechanical boundary condition appears to be recurrent in the experimental works reported in the literature such as those by Parekh et al. (2005), Chaudhuri et al. (2007) and by Bieling et al. (2016) in which growth occurs on a rigid support, be it glass or the tip of an atomic force microscope, in which both normal and tangential motions are inhibited. The latter constraint comes from the discrete number of fixed locations on the surface in which proteins promoting acting growth such as ActA are seeded.

The results of the clamped case may as well be applied to actin growing on the surface of spherical beads as reported e.g. in Cameron et al. (1999), Noireaux et al. (2000), van der Gucht et al. (2005). As discussed by Tomassetti et al. (2016), the stress field is not homogeneous in this case because growth at the surface of the sphere displaces outwards the previously grown rings, thus putting them in tension. However, at the surface of the rigid bead, one has $\lambda_1 = \lambda_2 = 1$ as in the case discussed here. Barring further and more detailed investigations, this case is expected to be always stable.

Mixed case. From Eq. (89), we obtain that in the frictionless rigid case, surface growth is stable as long as $\lambda_1 < 1/\lambda_{\text{Biot}} \simeq 1.84$, i.e. $\lambda_2 > \lambda_{\text{Biot}}$. The result is independent of $\bar{\pi}$. Given the relatively high value of stretch involved in the above threshold, it is expected that the frictionless rigid case, though not simple to realize in practice, be stable in most applications.

6. Surface tension

We argued in the previous section that steady state growth is stable only in the clamped case and mixed cases (see Eqs. (15) and (16)). Motivated by this result, we now generalize model by assuming that the boundary of the solid carries a constant energy σ per unit area in the current configuration. Alternatively, we may think of σ is the energy per unit length of a strip of unit depth.

We observe that when the clamping and mixed boundary conditions are enforced, the boundary of the body is a flat, and surface energy has no mechanical effect. Thus, we may limit our attention to the dead-load case. Taking advantage from the developments of the previous sections we shall point out only the differences with respect to the case with no surface energy.

The additional energetic contribution on the boundary results in a tangential surface tension (see for example Gurtin and Murdoch, 1975) which affects the traction condition. Precisely, (14) is replaced by

$$\mathbf{S}\mathbf{v} - \sigma\kappa\mathbf{n} = \mathbf{s}, \quad (93)$$

where λ is the stretch that a material fiber tangent to the referential boundary $\Gamma(t)$ undergoes when the body is deformed, and κ is the curvature of the deformed boundary $\gamma(t)$ (we remind the reader that \mathbf{n} and \mathbf{v} are, respectively, the normal in the current and in the reference configuration). These quantities are defined by

$$\lambda = |\mathbf{F}\boldsymbol{\tau}| \quad \text{and} \quad \kappa = \frac{d\mathbf{t}}{ds} \cdot \mathbf{n}, \quad (94)$$

where s is a measure of arc length over the deformed boundary $\gamma(t)$.

When the boundary $\Gamma(t)$ of the solid carries a surface energy density w , the expression (2b) of the driving force must be augmented by an additional contribution f_s . In the special case when this energy has the form $w(\lambda)$, such contribution reduces to Freund (1998), Fried and Gurtin (2003), Wu (1996) $f_s = (w(\lambda) - \lambda w'(\lambda))K$, where $K = \frac{\partial \boldsymbol{\tau}}{\partial s} \cdot \mathbf{v}$ is the curvature of $\Gamma(t)$. In the present case $w(\lambda) = \sigma\lambda$, thus the additional term vanishes. Summing up, with the exception of (93), the equations that govern the evolution problem in Section 2 are unchanged. In particular, (80) is still valid, although the actual value of the driving force is affected by surface tension, because of (93).

The treatment in Section 4 can be systematically repeated. The linearized bulk equations and kinetic equation, respectively, (32) and (33) are unchanged. However, the first of (34) is replaced by the linearization of (93):

$$\tilde{\Sigma}\mathbf{e}_2 - \lambda_2 \bar{T}_{11} \frac{\partial \tilde{\zeta}}{\partial \bar{x}_1} \mathbf{e}_1 - \sigma \frac{\partial^2}{\partial \bar{x}_1^2} (\lambda_2 \tilde{\zeta} + \tilde{u}_2) \mathbf{e}_2 = 0, \quad (95)$$

where the extra term on the right-hand side comes from the approximation

$$\kappa \simeq \frac{\partial^2}{\partial \bar{x}_1^2} (\lambda_2 \tilde{\zeta} + \tilde{u}_2), \quad (96)$$

which holds to within first order, as shown in Appendix A.

As in Section 5 we perform a change of independent and dependent variables (63)–(64). Note however that the problem has now a characteristic length scale, namely, the *elastocapillary length* (cf. Bico et al., 2018):

$$\ell = \frac{\sigma}{G}. \quad (97)$$

The only equation affected by surface tension is the projection of (95) along the \mathbf{e}_2 direction:

$$(\lambda_2^2 + \bar{\pi})u_{2,2} - q - \varepsilon(\lambda_2 \zeta_{,11} + u_{2,11}) = 0, \quad (98)$$

where we have set

$$\varepsilon = \frac{\ell}{L}. \quad (99)$$

As in Section 5, we eliminate q and ζ from (98) by making use of, respectively, (66b) and (68)₁, and then we express the displacement in terms of the stream function by making use of (69). The result is

$$(\lambda_1^2 - \bar{\pi}) \left[(1 + \lambda_1^4 + \bar{\pi}\lambda_1^2) \psi_{,112} + \psi_{,222} \right] + \varepsilon(\psi_{,1122} - \lambda_1^4 \psi_{,1111}) = 0. \quad (100)$$

Summing up, when surface tension comes into play, the linear system that governs small perturbations is given by the bulk equation (70), by the first of (71), and by (100). Of course, (100) reduces to (71)₂ for $\ell/L \rightarrow 0$.

Clearly, the equations obtained in the previous case are recovered in the limit $\varepsilon \rightarrow 0$, which corresponds to vanishing surface tension: $\sigma = 0$. The procedure leading to (80) can be repeated. The result is the following system:

$$\begin{bmatrix} \lambda_1 (1 + \bar{\pi}\lambda_1^2) \phi - 2\lambda_1^4 (\lambda_1^2 - \bar{\pi}) k & \lambda_1^3 (\lambda_1^2 + \bar{\pi}) \phi - \lambda_1^2 (1 + \lambda_1^4) (\lambda_1^2 - \bar{\pi}) k \\ (\lambda_1^2 - \bar{\pi}) \lambda_1^2 (\lambda_1^2 + \bar{\pi}) + (1 + \lambda_1^4) \varepsilon k & (\lambda_1^2 - \bar{\pi}) \lambda_1^2 (1 + \bar{\pi}\lambda_1^2) + 2\lambda_1^4 \varepsilon k \end{bmatrix} \begin{bmatrix} A \\ B \end{bmatrix} = \begin{bmatrix} 0 \\ 0 \end{bmatrix}. \quad (101)$$

Note that the first row of the above matrix coincides with the first row of the matrix in (80), which is obtained from the projection of the linearized traction condition along the horizontal direction. In fact, surface tension affects only the vertical component of the traction condition, which corresponds to the second row of (101).

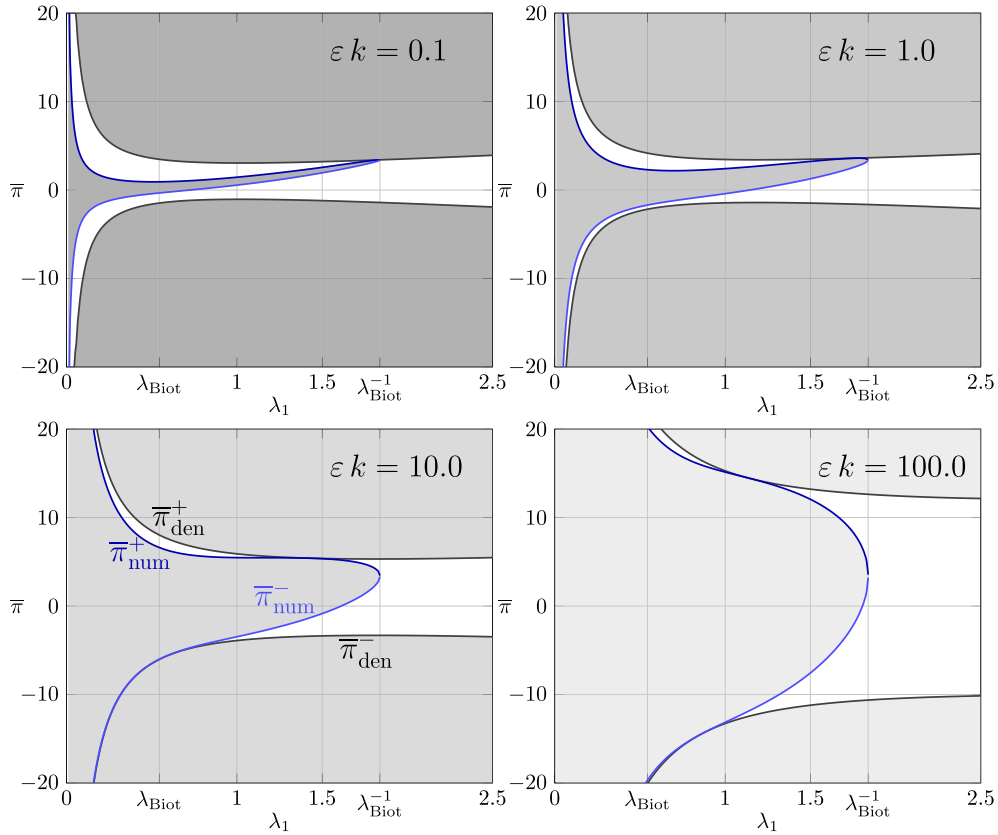


Fig. 11. Stability domains in the case with surface tension. Stable domains are shaded in gray. Lighter tones correspond to higher values of εk , i.e. to higher renormalized wavenumbers.

When the determinant of the above matrix is zero, non trivial solutions are obtained. That occurs when

$$\frac{\phi}{k} = \frac{(1 + \lambda_1^2) \lambda_1^2 (\bar{\pi} - \lambda_1^2)^2 - (1 + \lambda_1^2 + 3\lambda_1^4 - \lambda_1^6) \varepsilon k}{(1 + \lambda_1^2)^2 - \lambda_1^2 (\bar{\pi} - 1)^2 + (1 + \lambda_1^2) \varepsilon k} \cdot \frac{1}{\lambda_1} =: \Psi(\lambda_1, \bar{\pi}, \varepsilon k). \quad (102)$$

We shall refer to εk as the *renormalized wavenumber*.

We can now use (84) to express (102) in terms of the variables φ and K . We then recover (7) by taking the real part in (83).

6.1. Stability diagrams

In order to discuss the stability of the solution, we compute the values of $\bar{\pi}$ for which the numerator and denominator of (102), respectively, are zero:

$$\bar{\pi} = \bar{\pi}_{\text{num}}^{\pm}(\lambda_1, \varepsilon k) = \lambda_1^2 \pm \frac{1}{\lambda_1} \cdot \sqrt{\frac{1 + \lambda_1^2 + 3\lambda_1^4 - \lambda_1^6}{1 + \lambda_1^2} \cdot \varepsilon k} \quad \text{with} \quad 0 < \lambda_1 < \frac{1}{\lambda_{\text{Biot}}}, \quad (103)$$

$$\bar{\pi} = \bar{\pi}_{\text{den}}^{\pm}(\lambda_1, \varepsilon k) = 1 \pm \left(\lambda_1 + \frac{1}{\lambda_1} \right) \cdot \sqrt{1 + \frac{\varepsilon k}{1 + \lambda_1^2}}. \quad (104)$$

Functions $\bar{\pi}_{\text{num}}^+$ and $\bar{\pi}_{\text{den}}^+$ correspond to the plus sign in expressions (103) and (104), while $\bar{\pi}_{\text{num}}^-$ and $\bar{\pi}_{\text{den}}^-$ correspond to the expressions with the minus sign.

When $\varepsilon k = 0$, $\bar{\pi}_{\text{den}}^{\pm}$ coincides with the expression of $\bar{\pi}$ in Eq. (90), and $\bar{\pi}_{\text{num}}^{\pm}$ collapses into the curve $\bar{\pi} = \lambda_1^2$ depicted in Fig. 9. The stability domain coincides, as expected, with the one in Fig. 9.

For increasing values of the renormalized wave number εk , the stable domains are plotted in increasingly lighter shades of gray in Fig. 11. As in previous figures, white corresponds to unstable states. The following results are proven analytically by manipulating Eqs. (103), (104) and are as well noticeable in Fig. 11:

$$\lim_{\varepsilon k \rightarrow \infty} \bar{\pi}_{\text{num}}^{\pm}(\lambda_1, \varepsilon k) = \pm \infty \quad \forall \quad 0 < \lambda_1 < \frac{1}{\lambda_{\text{Biot}}} \quad (105a)$$

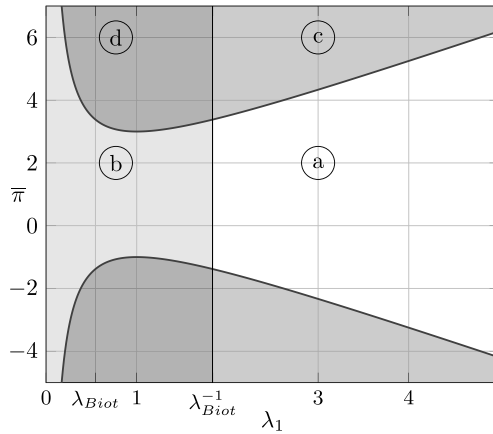


Fig. 12. The four regimes - a,b,c,d described in the text.

$$\lim_{\epsilon k \rightarrow \infty} \bar{\pi}_{\text{den}}^{\pm}(\lambda_1, \epsilon k) = \pm \infty \quad \forall \quad 0 < \lambda_1 \quad (105b)$$

$$\pm \bar{\pi}_{\text{num}}^{\pm}(\lambda_1, \epsilon k) \leq \pm \bar{\pi}_{\text{den}}^{\pm}(\lambda_1, \epsilon k) \quad \forall \quad 0 < \lambda_1 < \frac{1}{\lambda_{\text{Biot}}}, \quad \forall \quad 0 < \epsilon k \quad (105c)$$

Each of the above expressions is valid both with all \pm signs taking the + sign and with all \pm signs taking the - sign.

Based on the above results, four different stability regimes characterize the response of a biaxially loaded neo-Hookean slab subject to surface growth and surface tension. Each regime corresponds to a domain in the plane of parameters $\bar{\pi}$ and λ_1 which uniquely identifies the steady state configuration, as shown in Fig. 12.

a. Always unstable. Steady states with

$$\lambda_1 > 1/\lambda_{\text{Biot}} \quad \text{and} \quad \bar{\pi}_{\text{den}}^-(\lambda_1, 0) < \bar{\pi} < \bar{\pi}_{\text{den}}^+(\lambda_1, 0)$$

are unstable for all $k > 0$.

b. Stable for small wavelengths. For steady states with

$$\lambda_1 < 1/\lambda_{\text{Biot}} \quad \text{and} \quad \bar{\pi}_{\text{den}}^-(\lambda_1, 0) < \bar{\pi} < \bar{\pi}_{\text{den}}^+(\lambda_1, 0)$$

there exists a nondimensional wavenumber $k^*(\lambda_1, \bar{\pi})$ such that all perturbations with k larger than $k^*(\lambda_1, \bar{\pi})$ are stable, while the smaller ones are unstable.

c. Stable for large wavelengths. For steady states with

$$\lambda_1 > 1/\lambda_{\text{Biot}} \quad \text{and} \quad (\bar{\pi} < \bar{\pi}_{\text{den}}^-(\lambda_1, 0) \quad \text{or} \quad \bar{\pi} > \bar{\pi}_{\text{den}}^+(\lambda_1, 0))$$

there exists a nondimensional wavenumber $k^*(\lambda_1, \bar{\pi})$ such that all perturbations with k smaller than $k^*(\lambda_1, \bar{\pi})$ are stable, while the larger ones are unstable.

d. Stable for an intermediate interval of wavelengths. For steady states with

$$\lambda_1 > 1/\lambda_{\text{Biot}} \quad \text{and} \quad (\bar{\pi} < \bar{\pi}_{\text{den}}^-(\lambda_1, 0) \quad \text{or} \quad \bar{\pi} > \bar{\pi}_{\text{den}}^+(\lambda_1, 0))$$

there exist two nondimensional wavenumbers $k^-(\lambda_1, \bar{\pi})$ and $k^+(\lambda_1, \bar{\pi})$ such that all perturbations with k smaller than $k^-(\lambda_1, \bar{\pi})$ or larger than $k^+(\lambda_1, \bar{\pi})$ are stable, while the ones in between k^- and k^+ are unstable.

6.2. Discussion

Accounting for surface tension has generally the effect of making modes characterized by smaller wavelengths more stable. This is precisely what occurs in the case with surface tension and without surface growth presented in Appendix B.

The simultaneous presence of surface growth and surface tension instead presents some noteworthy aspects. First, there are four regimes instead of one, depending on the steady state configuration considered. Second, in no regime does there exist steady state configurations stable for all possible perturbed wavelengths. Finally, only one regime, namely “b. Stable for small wavelengths”, is consistent with what is observed in Appendix B in the absence of surface growth.

Declaration of competing interest

The authors declare that they have no known competing financial interests or personal relationships that could have appeared to influence the work reported in this paper.

Acknowledgments

R.A. and E.P. gratefully acknowledge the support of the MIT-FVG Seed Fund. The work of G.T. and E.P. was supported by the Italian PRIN 2017 project “Mathematics of active materials: From mechanobiology to smart devices”. G.T. and E.P. thankfully acknowledge the support of the Italian National Group of Mathematical Physics (GNFM-INdAM). G.T. acknowledges the Grant of Excellence Departments, MIUR, Italian Ministry of University and Research (Art.1, commi 314 – 337, Legge 232/2016).

Appendix A. Proof of Eq. (96)

In this section we derive the expression (96) for the curvature of the boundary $\gamma(t)$ in the perturbed state. Since time plays no role, we omit the dependence on t in the following calculations. The function

$$\gamma(\bar{\xi}_1) = \mathbf{x}(\bar{\xi}_1, \bar{\zeta} + \tilde{\zeta}(\bar{\xi}_1)) \quad (\text{A.1})$$

is a parametrization of the set $\gamma(t)$, the boundary of $\omega(t)$. Then,

$$\begin{aligned} \gamma(\bar{\xi}_1) &\simeq \mathbf{x}(\bar{\xi}_1, \bar{\zeta}) + \frac{\partial \mathbf{x}}{\partial \bar{\xi}_2}(\bar{\xi}_1, \bar{\zeta}) \tilde{\zeta}(\bar{\xi}_1) \\ &\stackrel{(30)}{=} \underbrace{\bar{\mathbf{x}}(\bar{\xi}_1, \bar{\zeta})}_{\text{order 0}} + \underbrace{\tilde{\mathbf{u}}(\bar{\xi}_1, \bar{\zeta}) + \frac{\partial \bar{\mathbf{x}}}{\partial \bar{\xi}_2}(\bar{\xi}_1, \bar{\zeta}) \tilde{\zeta}(\bar{\xi}_1)}_{\text{order 1}} + \underbrace{\frac{\partial \tilde{\mathbf{u}}}{\partial \bar{\xi}_2}(\bar{\xi}_1, \bar{\zeta}) \tilde{\zeta}(\bar{\xi}_1)}_{\text{higher order}}, \end{aligned} \quad (\text{A.2})$$

where $\bar{\mathbf{x}}$ is the deformation in the reference state. By (18a), we have

$$\frac{\partial \bar{\mathbf{x}}}{\partial \bar{\xi}_1} \simeq \bar{\mathbf{F}} \mathbf{e}_1 = \lambda_1 \mathbf{e}_1 \quad \frac{\partial \bar{\mathbf{x}}}{\partial \bar{\xi}_2} = \bar{\mathbf{F}} \mathbf{e}_2 = \lambda_2 \mathbf{e}_2 = \lambda_1^{-1} \mathbf{e}_2, \quad (\text{A.3})$$

and

$$\gamma' = \lambda_1 \mathbf{e}_1 + \frac{\partial \tilde{\mathbf{u}}}{\partial \bar{\xi}_1} + \lambda_1^{-1} \frac{\partial \tilde{\zeta}}{\partial \bar{\xi}_1} \mathbf{e}_2 = \lambda_1 \mathbf{e}_1 + \underbrace{\frac{\partial}{\partial \bar{x}_1}(\lambda_1 \tilde{\mathbf{u}} + \tilde{\zeta} \mathbf{e}_2)}_{\tilde{\gamma}'}. \quad (\text{A.4})$$

To within first order, we have $|\gamma'| \simeq \lambda_1$, hence the tangent vector at the boundary is

$$\mathbf{t} = \frac{\gamma'}{|\gamma'|} \simeq \mathbf{e}_1 + \lambda_1^{-1} (\tilde{\gamma}' \cdot \mathbf{e}_2) \mathbf{e}_2 = \mathbf{e}_1 + \frac{\partial}{\partial \bar{x}_1} (\tilde{u}_2 + \lambda_2 \tilde{\zeta}) \mathbf{e}_2, \quad (\text{A.5})$$

and the normal vector is

$$\mathbf{n} \simeq \mathbf{e}_2 - \frac{\partial}{\partial \bar{x}_1} (\tilde{u}_2 + \lambda_2 \tilde{\zeta}) \mathbf{e}_1. \quad (\text{A.6})$$

The parameter $\bar{\xi}_1$ and the arc-length coordinate s are related by

$$\frac{ds}{d\bar{\xi}_1} = |\gamma'| \simeq \lambda_1, \quad (\text{A.7})$$

hence the curvature in the current configuration can be approximated as

$$\kappa = \frac{d\mathbf{t}}{ds} \cdot \mathbf{n} \simeq \lambda_1^{-1} \frac{d\mathbf{t}}{d\bar{\xi}_1} \cdot \mathbf{n} = \frac{d\mathbf{t}}{d\bar{x}_1} \cdot \mathbf{n} \simeq \frac{\partial^2}{\partial \bar{x}_1^2} (\tilde{u}_2 + \lambda_2 \tilde{\zeta}). \quad (\text{A.8})$$

The last term is the right-hand side of (96).

Appendix B. Biot's surface instability problem with dead load and surface tension

In this section Biot's surface instability problem without surface growth is presented in an extended version with vertical dead load and surface tension. The results bear interesting analogies and differences with those presented in the main body of this paper.

The fundamental equilibrium configuration is identical to the one presented in Section 3 for the dead load case with the difference that the boundaries $\bar{\Gamma}$ and $\bar{\gamma}$ are independent of time t . The stress state is biaxial. Given that $\bar{\Gamma}$ and $\bar{\gamma}$ are flat, surface tension affects only the perturbed configuration.

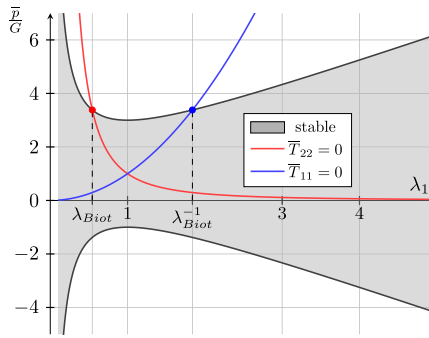


Fig. B.13. Stability domains in the $\lambda_1 - \bar{\pi}$ plane for the dead load case without both surface growth and surface tension.

B.1. Linear stability analysis

The linear stability analysis is characterized by bulk equations coincident with (66). The boundary conditions read

$$\Sigma_{12} = 0 \iff \lambda_2^2 u_{1,2} + \bar{\pi} u_{2,1} = 0 \quad (\text{B.1a})$$

$$\Sigma_{22} = 0 \iff (\lambda_2^2 + \bar{\pi}) u_{2,2} - q = \varepsilon u_{2,11} \quad (\text{B.1b})$$

where $u_{2,11}$ is the non dimensional curvature in the current, perturbed configuration. The introduction of a stream function ψ by means of (69) leads again to the partial differential equation (70) in the bulk for ψ , while boundary conditions (B.1) lead to

$$\psi_{,22} - \lambda_1^2 \cdot \bar{\pi} \cdot \psi_{,11} = 0 \quad (\text{B.2a})$$

$$(\lambda_1^4 + \lambda_1^2 \bar{\pi} + 1) \psi_{,211} + \psi_{,222} = \varepsilon \lambda_1^2 \psi_{,1111} \quad (\text{B.2b})$$

Substituting the Ansatz

$$\psi(x_1, x_2, \tau) = h(y) g(\tau) e^{ikx_1}, \quad \text{with } y = k x_2 \quad (\text{B.3})$$

into (70), one finds again the same expression for $h(y)$ as in (77). The linear system

$$\begin{bmatrix} 1 + \lambda_1^2 \bar{\pi} & \lambda_1^2 (\lambda_1^2 + \bar{\pi}) \\ \lambda_1^2 + \bar{\pi} + \varepsilon k & 1 + \lambda_1^2 \bar{\pi} + \varepsilon k \end{bmatrix} \begin{bmatrix} A \\ B \end{bmatrix} = \begin{bmatrix} 0 \\ 0 \end{bmatrix} \quad (\text{B.4})$$

is then obtained when inserting (B.3) into (B.2). Non trivial solutions are only possible when the determinant of the coefficient matrix in (B.4) is zero, i.e. when

$$(1 - \lambda_1^2) \cdot \left((1 + \lambda_1^2)^2 - \lambda_1^2 (\bar{\pi} - 1)^2 + (1 + \lambda_1^2) \varepsilon k \right) = 0. \quad (\text{B.5})$$

The second factor in Eq. (B.5) above coincides with the denominator of Eq. (102) obtained in the case with surface growth. The solutions for several specific cases as well as the most general one are discussed below.

B.2. Results for the case with surface tension and no dead load

The case without dead load, i.e. $\bar{T}_{22} = 0$, corresponds to $\bar{\pi} = 1/\lambda_1^2$ according to (28). The determinant in Eq. (B.5) is zero when either $\lambda_1 = 1$ or when the polynomial $\lambda_1^6 + \lambda_1^4(1+k) + \lambda_1^2(3+k) - 1$ has a root. For $k = 0$, the root coincides with λ_{Biot} , then it decreases monotonically to zero for $k \rightarrow \infty$. Thus the stable domain widens for larger wave numbers. As expected, surface tension has a stabilizing effect on smaller wavelengths. In fact, the smaller the wavelength, the smaller the λ_1 threshold needed for that mode to occur.

B.3. Results for the case with dead load and no surface tension

The case without surface tension corresponds to the choice $k = 0$ in (B.5). Non trivial solutions are possible when the threshold for $\bar{\pi}$ in Eq. (90) is attained. The result is analogous to the one with surface growth in Section 5.4 with the main difference that the stable domain is now the complement of the one shaded in gray in Fig. 9. Another difference with respect to Section 5.4 is that therein threshold (90) represents a singularity of the exponent φ , while in the present case the determinant is equal to zero and continuous at the threshold line given by (90). Looking at Fig. B.13, the red curve corresponds to the absence of dead load, i.e. $\bar{T}_{22} = 0$. In that case non trivial solutions are possible when $\lambda_1 = \lambda_{\text{Biot}}$. The blue curve corresponds to the case of dead load without lateral confinement, i.e. $\bar{T}_{11} = 0$, for which stability is lost when $\lambda_1 = 1/\lambda_{\text{Biot}}$.

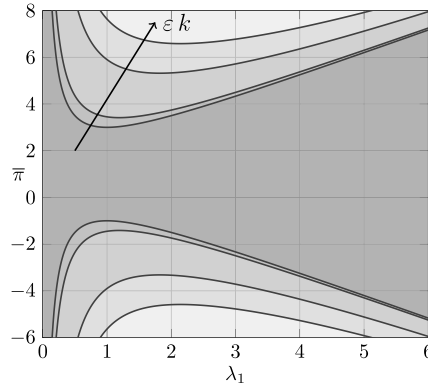


Fig. B.14. Dead load case with surface tension and without surface growth. Stability domains in the $\lambda_1 - \bar{\pi}$ plane for $\varepsilon k = 0, 1, 10, 20$.

B.4. Results for the case with surface tension and dead load

In the most general case, non trivial solutions are attained when $\bar{\pi}$ is given by the expression (104) as a function of λ_1 and εk . The evolution of the stability domain is shown in Fig. B.14 for increasing values of εk , namely 0, 1, 10 and 20. As for the case without dead load in Appendix B.2 and as expected when accounting for surface tension, the smaller the wavelength, the larger the stability domain. Considering the difference with respect to the case with surface growth in Section 6, we notice again that whilst with surface growth exponent φ is singular at the threshold (104) and the stable domain is beyond it, in the present case without surface growth, the determinant is equal to zero and continuous at (104) and the stable domain is below the threshold line.

Appendix C. Proof of inequality (105c)

We set out to prove that

$$+\bar{\pi}_{\text{num}}^+(\lambda_1, \varepsilon k) \leq +\bar{\pi}_{\text{den}}^+(\lambda_1, \varepsilon k) \quad \forall \quad 0 < \lambda_1 < \frac{1}{\lambda_{\text{Biot}}}, \quad \forall \quad \varepsilon k > 0. \quad (\text{C.1})$$

The proof that $\bar{\pi}_{\text{num}}^-$ is above $\bar{\pi}_{\text{den}}^-$ is analogous.

For convenience, let us introduce the following rational expressions of λ_1 and εk

$$a = \lambda_1^3; \quad b = \lambda_1^3; \quad c = \frac{1 + \lambda_1^2 + 3\lambda_1^4 - \lambda_1^6}{1 + \lambda_1^2} \varepsilon k; \quad d = (1 + \lambda_1^2)(1 + \lambda_1^2 + \varepsilon k) \quad (\text{C.2})$$

such that

$$\lambda_1 \bar{\pi}_{\text{num}}^+ = b + \sqrt{c}; \quad \lambda_1 \bar{\pi}_{\text{den}}^+ = a + \sqrt{d}. \quad (\text{C.3})$$

The thesis is then equivalent to proving that $b - a \leq \sqrt{d} - \sqrt{c}$. It turns out that $\sqrt{d} - \sqrt{c}$ is always non negative since

$$d - c = (1 + \lambda_1^2)^2 + \frac{\lambda_1^2(1 - \lambda_1^2)^2}{1 + \lambda_1^2} \varepsilon k \geq 0 \quad (\text{C.4})$$

Then (105c) holds for $\lambda_1 < 1$ since $b - a$ is negative in that range and hence smaller than $\sqrt{d} - \sqrt{c}$. To prove that (105c) holds also for $0 < \lambda_1 < \frac{1}{\lambda_{\text{Biot}}}$, both positive sides of the inequality are squared.

$$(\sqrt{d} - \sqrt{c})^2 - (b - a)^2 = \left(\sqrt{(1 + \lambda_1^2 + 3\lambda_1^4 - \lambda_1^6) \left(1 + \frac{\varepsilon k}{1 + \lambda_1^2}\right)} - \sqrt{(1 + \lambda_1^2)\varepsilon k} \right)^2 \quad (\text{C.5})$$

Eq. (C.5) above shows that the difference of the square of each side is always non negative, hence (105c) holds.

References

- Abeyaratne, R., Puntel, E., Tomassetti, G., 2020. Treadmilling stability of a one-dimensional actin growth model. *Int. J. Solids Struct.* 198, 87–98. <http://dx.doi.org/10.1016/j.ijsolstr.2020.04.009>.
- Abeyaratne, R., Purohit, P.K., 2020. A continuum model for the growth of dendritic actin networks. *Proc. R. Soc. A Math. Phys. Eng. Sci.* 476 (2241), 20200464. <http://dx.doi.org/10.1098/rspa.2020.0464>.
- Ambrosi, D., Ateshian, G., Arruda, E., Cowin, S., Dumais, J., Goriely, A., Holzapfel, G., Humphrey, J., Kemkemer, R., Kuhl, E., Olberding, J., Taber, L., Garikipati, K., 2011. Perspectives on biological growth and remodeling. *J. Mech. Phys. Solids* 59 (4), 863–883. <http://dx.doi.org/10.1016/j.jmps.2010.12.011>, URL: <https://linkinghub.elsevier.com/retrieve/pii/S0022509610002516>.

- Ambrosi, D., Preziosi, L., Vitale, G., 2012. The interplay between stress and growth in solid tumors. *Mech. Res. Commun.* 42, 87–91. <http://dx.doi.org/10.1016/j.mechrescom.2012.01.002>, URL: <https://linkinghub.elsevier.com/retrieve/pii/S0093641312000043>.
- Bico, J., Reyssat, É., Roman, B., 2018. Elastocapillarity: When surface tension deforms elastic solids. *Annu. Rev. Fluid Mech.* 50 (1), 629–659. <http://dx.doi.org/10.1146/annurev-fluid-122316-050130>, URL: <https://www.annualreviews.org/doi/10.1146/annurev-fluid-122316-050130>.
- Bieling, P., Li, T.-D., Weichsel, J., McGorty, R., Jreij, P., Huang, B., Fletcher, D.A., Mullins, R.D., 2016. Force feedback controls motor activity and mechanical properties of self-assembling branched actin networks. *Cell* 164 (1), 115–127. <http://dx.doi.org/10.1016/j.cell.2015.11.057>.
- Biot, M.A., 1963. Surface instability of rubber in compression. *Appl. Sci. Res. Sect. A* 12 (2), 168–182. <http://dx.doi.org/10.1007/BF03184638>.
- Cameron, L.A., Footer, M.J., van Oudenaarden, A., Theriot, J.A., 1999. Motility of acta protein-coated microspheres driven by actin polymerization. *Proc. Natl. Acad. Sci. USA* 96 (9), 4908–4913. <http://dx.doi.org/10.1073/pnas.96.9.4908>.
- Cardamone, L., Laio, A., Torre, V., Shahapure, R., DeSimone, A., 2011. Cytoskeletal actin networks in motile cells are critically self-organized systems synchronized by mechanical interactions. *Proc. Natl. Acad. Sci. USA* 108 (34), 13978–13983. <http://dx.doi.org/10.1073/pnas.1100549108>.
- Chaudhuri, O., Parekh, S.H., Fletcher, D.A., 2007. Reversible stress softening of actin networks. *Nature* 445, 295–298. <http://dx.doi.org/10.1038/nature05459>.
- Dafalias, Y.F., Panayotounakos, D.E., Pitouras, Z., 2008. Stress field due to elastic mass growth on spherical and cylindrical substrates. *Int. J. Solids Struct.* 45, 4629–4647. <http://dx.doi.org/10.1007/s10237-007-0113-y>.
- de Buyl, P., Mikhailov, A.S., Kapral, R., 2013. Self-propulsion through symmetry breaking. *Europhys. Lett.* 103 (6), 60009. <http://dx.doi.org/10.1209/0295-5075/103/60009>.
- Erllich, A., Moulton, D.E., Goriely, A., 2019. Are homeostatic states stable? Dynamical stability in morphoelasticity. *Bull. Math. Biol.* 81 (8), 3219–3244. <http://dx.doi.org/10.1007/s11538-018-0502-7>, URL: <http://link.springer.com/10.1007/s11538-018-0502-7>.
- Freund, L., 1998. A surface chemical potential for elastic solids. *J. Mech. Phys. Solids* 46 (10), 1835–1844. [http://dx.doi.org/10.1016/S0022-5096\(98\)00019-2](http://dx.doi.org/10.1016/S0022-5096(98)00019-2).
- Fried, E., Gurtin, M.E., 2003. The role of the configurational force balance in the nonequilibrium epitaxy of films. *J. Mech. Phys. Solids* 51 (3), 487–517. [http://dx.doi.org/10.1016/S0022-5096\(02\)00077-7](http://dx.doi.org/10.1016/S0022-5096(02)00077-7).
- Fu, Y., Ogden, R., 1999. Nonlinear stability analysis of pre-stressed elastic bodies. *Contin. Mech. Thermodyn.* 11 (3), 141–172. <http://dx.doi.org/10.1007/s001610050108>, URL: <http://link.springer.com/10.1007/s001610050108>.
- Garcia, K.E., Kroenke, C.D., Bayly, P.V., 2018. Mechanics of cortical folding: stress, growth and stability. *Philos. Trans. R. Soc. B* 373 (1759), 20170321. <http://dx.doi.org/10.1098/rstb.2017.0321>, URL: <https://royalsocietypublishing.org/doi/10.1098/rstb.2017.0321>.
- Gei, M., Ogden, R.W., 2002. Vibration of a surface-coated elastic block subject to bending. *Math. Mech. Solids* 7 (6), 607–628. <http://dx.doi.org/10.1177/108128602029657>.
- Gurtin, M.E., Murdoch, I.A., 1975. A continuum theory of elastic material surfaces. *Arch. Ration. Mech. Anal.* 57 (4), 291–323. <http://dx.doi.org/10.1007/BF00261375>, URL: <http://link.springer.com/10.1007/BF00261375>.
- John, K., Peyla, P., Kassner, K., Prost, J., Misbah, C., 2008. Nonlinear study of symmetry breaking in actin gels: Implications for cellular motility. *Phys. Rev. Lett.* 100 (6), 068101. <http://dx.doi.org/10.1103/PhysRevLett.100.068101>.
- Li, B., Cao, Y.-P., Feng, X.-Q., Gao, H., 2012. Mechanics of morphological instabilities and surface wrinkling in soft materials: a review. *Soft Matter* 8 (21), 5728. <http://dx.doi.org/10.1039/c2sm00011c>, URL: <http://xlink.rsc.org/?DOI=c2sm00011c>.
- Noireaux, V., Golsteyn, R.M., Friederich, E., Prost, J., Antony, C., Louvard, D., Sykes, C., 2000. Growing an actin gel on spherical surfaces. *Biophys. J.* 78 (3), 1643–1654. [http://dx.doi.org/10.1016/S0006-3495\(00\)76716-6](http://dx.doi.org/10.1016/S0006-3495(00)76716-6).
- Parekh, S.H., Chaudhuri, O., Theriot, J.A., Fletcher, D.A., 2005. Loading history determines the velocity of actin-network growth. *Nature Cell Biol.* 7 (12), 1219–1223. <http://dx.doi.org/10.1038/ncb1336>, URL: <http://www.nature.com/doi/10.1038/ncb1336>.
- Prost, J., Joanny, J.-F., Lenz, P., Sykes, C., 2008. The physics of listeria propulsion. In: Lenz, P. (Ed.), *Cell Motility. In: Biological and Medical Physics, Biomedical Engineering*, Springer, New York, NY, pp. 1–30. http://dx.doi.org/10.1007/978-0-387-73050-9_1.
- Tallinen, T., Biggins, J.S., Mahadevan, L., 2013. Surface sulci in squeezed soft solids. *Phys. Rev. Lett.* 110 (2), 024302. <http://dx.doi.org/10.1103/PhysRevLett.110.024302>, URL: <https://link.aps.org/doi/10.1103/PhysRevLett.110.024302>.
- Tomassetti, G., Cohen, T., Abeyaratne, R., 2016. Steady accretion of an elastic body on a hard spherical surface and the notion of a four-dimensional reference space. *J. Mech. Phys. Solids* 96, 333–352. <http://dx.doi.org/10.1016/j.jmps.2016.05.015>.
- van der Gucht, J., Paluch, E., Plastino, J., Sykes, C., 2005. Stress release drives symmetry breaking for actin-based movement. *Proc. Natl. Acad. Sci. USA* 102 (22), 7847. <http://dx.doi.org/10.1073/pnas.0502121102>.
- Wu, C.H., 1996. The chemical potential for stress-driven surface diffusion. *J. Mech. Phys. Solids* 44 (12), 2059–2077. [http://dx.doi.org/10.1016/S0022-5096\(96\)00059-2](http://dx.doi.org/10.1016/S0022-5096(96)00059-2).